Environmental Science Advances

ROYAL SOCIETY OF CHEMISTRY

PAPER

View Article Online
View Journal | View Issue

Cite this: *Environ. Sci.: Adv.*, 2026, **5**, 257

Tropospheric carbon dioxide and methane temporal variability using atmospheric infrared sounding data: a case study of Pakistan

Bahadar Zeb,*[a] Khan Alam,[b] Allah Ditta,*[c] Mazhar Sajjad[d] and Maqbool Ahmad[e]

Rising levels of carbon dioxide (CO_2) and methane (CH_4) in the atmosphere are significant contributors to global climate change, although regional differences and mechanisms are poorly understood, especially in South Asia. This study examines the spatial and temporal patterns, seasonal changes, and climatic effects of CO_2 and CH_4 over Pakistan through satellite measurements (AIRS, 2002–2017), weather, and vegetation indicators (NDVI). We evaluate the contribution of human-made activities, biomass burning, and natural processes (*e.g.*, monsoon or soil respiration) to the regulation of greenhouse gas (GHG) concentrations. Moreover, we assess the contribution of long-range transportation by our neighboring areas (the Middle East and Central Asia) using HYSPLIT trajectory modeling. The results show an average yearly growth of CO_2 (2.1 ppm per year) and CH_4 (3.5 ppb per year), seasonal peaks of CO_2 (spring) and CH_4 (summer), associated with agriculture, temperature-dependent respiration, and monsoonal cycles. CO_2 and NDVI (−0.50) and CH_4 and NDVI (+0.64) depict negative and positive associations, respectively, and play the role of vegetation as a carbon sink and wetland and rice paddy emissions. Other significant findings of the study are sudden changes in GHG patterns (CO_2: 2009; and CH_4: 2007–2014) that occur with upward temperatures, indicating climate feedbacks. This study incorporates radiative forcing dynamics and air mass paths, which provide important insights into the regional GHG drivers and their climatic implications and contribute to policy interventions to reduce emission levels in South Asia. The cloud fraction had a negative correlation with both CO_2 ($r = -0.36$ and $p < 0.04$) and CH_4 ($r = -0.20$ and $p < 0.03$). The trajectories of the air mass of the rear indicate that the distant pollution of neighboring countries is a factor. Burning of crop residues, car emissions, forest burning, and others release small quantities of gases and contaminants into the air. This study compares atmospheric CO_2 and CH_4 prediction models. The dominant trend is strong linearity. In the case of CH_4, linear regression is the best and most suggested model. In the case of CO_2, ARIMA provided the most accurate forecasts by detecting minor autocorrelation. More complicated models, such as LSTM, failed to work, which proved that simpler models are effective on this kind of data.

Received 17th September 2025
Accepted 12th November 2025

DOI: 10.1039/d5va00327j

rsc.li/esadvances

Environmental significance

Among greenhouse gases, carbon dioxide (CO_2) and methane (CH_4) are the most important gases that have a significant impact on the climate. The current study was conducted to examine the monthly and seasonal variation in the concentrations of CO_2 and CH_4, to better understand the inter-annual variation as well as increasing trends of CO_2 and CH_4 during the study period (2002–2017), to identify the time-varying characteristics of CO_2 and CH_4 concentrations and the probable causes, which characterize the variability in different time scales over Pakistan, and to investigate the effects of meteorology, cloud properties, vegetation dynamics on CO_2 and CH_4 concentrations and the effects of long-range air masses on CO_2 and CH_4 concentrations. The results show that the CO_2 and CH_4 emission levels in Pakistan are alarming and ultimately contribute to climate change. It is expected that these results will help scientific communities further explore the root causes of the recent CO_2 and CH_4 increase to better mitigate their potential impact on global warming.

[a]*Department of Mathematics, Shaheed Benazir Bhutto University, Sheringal Dir (Upper), Khyber Pakhtunkhwa, Pakistan. E-mail: zebsbbu@gmail.com*
[b]*Department of Physics, University of Peshawar, Khyber Pakhtunkhwa, Pakistan*
[c]*Department of Environmental Sciences, Shaheed Benazir Bhutto University Sheringal, Dir (U), Khyber Pakhtunkhwa 18000, Pakistan. E-mail: allah.ditta@sbbu.edu.pk*
[d]*Department of Computer Science, Alhamd Islamic University, Islamabad, Pakistan*
[e]*Department of Elementary and Secondary Education, Peshawar, Khyber Pakhtunkhwa, Pakistan*

Introduction

With the increasing awareness of climate change, many solutions have been suggested to address this issue.[1,2] Decades of studies have proven that there is a strong association between increasing GHG levels and climate change.[3,4] The greatest pollutants of global warming are carbon dioxide (CO_2) and methane (CH_4).[5]

The energy sector is the largest emitter of GHGs, followed by agriculture. The life cycle of their emissions can vary substantially, ranging between several years and millennia, yet their cumulative effect is the cause of climate change over long periods.[2] The main sources of CO_2 emissions are the combustion of fossil fuels, the manufacturing of cement, and changes in land use, and they are ultimately eliminated by land and ocean sinks. According to Le Querre *et al.*,[6] forty-five percent of the world's CO_2 emissions were held up in the atmosphere, with the rest being absorbed by land (30%) and ocean (24%) between 1959 and 2017. CO_2, a major greenhouse gas (GHG), is important in the maintenance of a balance in the temperature of the Earth as well as in the process of climate change.[7] It also contributes to important biological processes like photosynthesis and respiration.[2] Nevertheless, human actions, especially industrialization, have increased the CO_2 levels in the atmosphere from 280 ppm to over 416 ppm within the last 150 years.[8] This elevation has greatly changed global radiative forcing, which has led to escalating climatic change.[2] To curb further rise in global temperatures, minimizing CO_2 emissions should be a major priority. Some of the strategies that will help include a shift to using fossil fuels, increasing carbon sequestration, and sustainable land use. The most active greenhouse gas, second in importance after carbon dioxide (CO_2) in the atmosphere, is methane (CH_4).

Even though methane is less concentrated than CO_2, it has a high global warming potential. Human activities have significantly increased their atmospheric concentration, which is now higher than that before the industrial era. Methane is produced during both natural and anthropogenic activities and is grouped into three formation pathways: (1) Thermogenic: it is formed under high pressure and temperature at very deep levels in the crust of the earth as a result of decomposing organic matter. It is emitted during the extraction, transportation, and processing of fossil fuels (oil, gas, and coal). (2) Pyrogenic: it is formed by the partial decomposition of organic matter, such as wildfires and savanna burning, agricultural waste and crop residue burning, and biofuel combustion.[9] (3) Microbial: it is formed by methanogenic bacteria in anaerobic environments, including natural wetlands (lakes, peatlands, and rice paddies); livestock digestion (ruminants); landfills; and wastewater treatment. Although methane is inexhaustible, it undergoes (1) oxidation by hydroxyl radicals (OH) (approximately 90 percent of the removal) to produce other types of secondary pollutants, such as formaldehyde (CH_2O), carbon monoxide (CO), and ozone (O_3);[10] (2) absorption by the soil (oxidation of dry soil); and (3) chlorination under the influence of chlorofluorocarbons (CFCs). Total methane emissions are currently more than what nature has taken up; thus, there is a progressive rise in concentrations present in the atmosphere. The main cause of this increase is human activities, which include the consumption of fossil fuels, farming, and waste disposal.[2] It has been demonstrated that, globally, several studies have been used to estimate and describe the rising patterns and variability of CO_2 and CH_4 using satellites. Studies based on the measurements of instruments, such as the Greenhouse gases Observing Satellite (GOSAT) and the Orbiting Carbon Observatory-2 (OCO-2), have provided previously unknown details on the spatial and temporal distribution of these gases and found continuing increases in atmospheric levels.[11] Major emission hotspots, including the industrialized areas of East Asia and North America, and large natural sources, such as the Amazon basin, were identified. Moreover, global studies have played a key role in explaining the multifaceted relationship between human-generated emissions, natural biogeochemical cycles, and climatic factors, like temperature and precipitation, which give rise to seasonal and interannual changes.[6,12] It is against this global body of work that regional studies, including this one, can be compared and contextualized. The report by IPCC[2] indicates that the levels of CO_2 and CH_4 in the atmosphere have been rising since the Industrial Revolution. Nevertheless, most developing nations find it difficult to keep regular track of such gases owing to a lack of know-how and state-of-the-art apparatus. Long-term greenhouse gas (GHG) evaluation requires ground-based measurements in most cases. Remote sensing through satellites is a possible solution. Although the spatial resolution can be low, this technology can provide continuous global results for trace gases, providing essential data on their trends and effects on human health, ecosystems, and climate change. Remote sensing as a state-of-the-art methodology supplements ground-based state-of-the-art systems and improves the capacity to monitor GHG emissions to guide mitigation strategies.

Pakistan is one of the largest greenhouse gas (GHG) emitters in the world, with the 13th largest global anthropogenic emission of CH_4, and 504.59 million tons of total emissions in 2018.[13] Key concerns are as follows: (1) large amounts of methane (CH_4) emissions: 13th largest anthropogenic CH_4 emitter globally and top 5 in livestock-related CH_4 emissions (enteric fermentation); (2) CO_2 build-up: deforestation, and local sources of great emission sources are as follows: transportation (vehicles), agriculture (livestock and biomass burning), and forest fires. Pakistan experiences aggravated floods, droughts, and extreme temperatures. Developing countries, like Pakistan, have inadequate mechanisms to even monitor such emissions due to the high cost of deploying ground-based monitoring networks. However, with the latest developments in the field of atmospheric remote sensing (RS), reliable sensors, such as the atmospheric infrared sounder (AIRS), have made monitoring of CO_2 and CH_4 feasible.[13,14] Mahmood *et al.*[15] investigated the atmospheric concentrations of CO_2 and CH_4 over Pakistan using the Atmospheric Infrared Sounder (AIRS) from 2010 to 2015. Ning An *et al.*[16] attempted to evaluate the potential of space-based observations to monitor atmospheric CO_2 changes over 120 districts through simple data-driven analyses from 2015 to 2020. Noman *et al.*[17] estimated the GHG (carbon dioxide and methane) footprint based on the one-year average fossil fuel consumption in selected Private Sector Universities of Karachi.

Although some previous studies have provided snapshots, these are usually constrained by more stringent periods or a more focused consideration. This study fills this gap by providing a long-term (16 years) analysis of both CO_2 and CH_4 across Pakistan. The originality of this work is an approach that is an integrated analysis of the spatiotemporal trends of interest and study of the driving mechanism, *i.e.*, the importance of meteorological parameters (temperature, humidity,

precipitation, and wind speed), vegetation dynamics (NDVI), and cloud characteristics, and a critical evaluation of the transportation of transboundary pollution through HYSPLIT modelling. This complex analysis offers a more comprehensive explanation of the causes of GHG variability in this poorly studied but noteworthy area. Regrettably, the successful application of satellite RS in investigating CO_2 and CH_4 monitoring in Pakistan has hardly been documented. Thus, this research is aimed at tracing the temporal distribution patterns of CO_2 and CH_4 in the long term (2002–2017) in Pakistan and predicting the two gases using AIRS data. The results will be used to make the scientific community aware of the factors that cause the increase in CO_2 and CH_4 in the air and to overcome their contribution to global warming. This study points to an alarming level of emissions of these gases in Pakistan, which has contributed to climate change.

Experimental

Description of the study area and its meteorological conditions

Pakistan is located in South Asia and is bordered by India to the east, Afghanistan and Iran to the west, China to the north, and the Arabian Sea to the south. It lies between Longitude: 60°50′ E to 77°50′ E, Latitude: 23°35′ N to 37°05′ N, covering an area of approximately 881 913 square kilometres (Fig. 1 and Table 1). The country boasts a variety of landscapes with the high mountain ranges of the Himalayan and Karakoram ranges located in the north, the fertile Indus River plains located in the central region, and the arid deserts of Sindh and Baluchistan located in the south and west. Pakistan has great climatic diversity, with an alpine climate in the highlands of the country and arid and semi-arid climates in the southern plains. There are four seasons in the country: cool winter (December–February), spring (March–May), summer (June–August), and autumn (September–November).[18] The Indus River is the lifeblood of Pakistan, and the problems of water shortage and climate change are increasing. Pakistan is governed by four provinces: Punjab, Sindh, Khyber Pakhtunkhwa (KP), and Baluchistan, and the federally governed territory of Islamabad Capital Territory, Azad Jammu and Kashmir, and Gilgit-Baltistan. Pakistan is the fifth most populous nation in the world, with a population of over 240 million people. Urban centres, like Karachi, Lahore, and Islamabad, are the centre of economic, political, and cultural activities, with rural life in most cases being agrarian. This area is of interest to the study as it is important in terms of the ecological zones and socioeconomic inequalities and is prone to environmental and

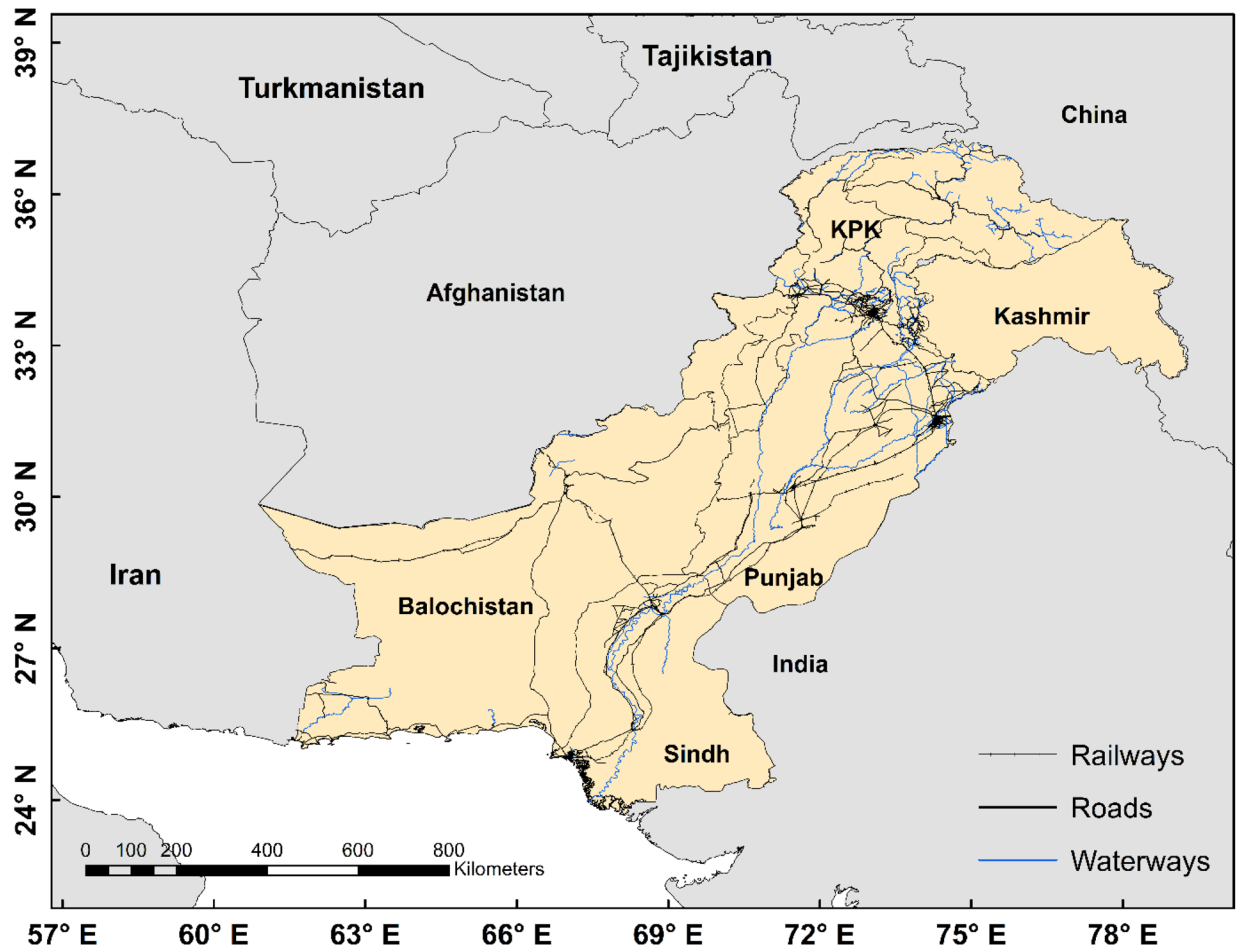

Fig. 1 Map of the study area (ArcMap 10.5). All the datasets (shapefiles) were obtained from DIVA GIS and UNOCHA.

Table 1 Summary of the annual meteorological aspects

Parameter	Annual pattern and key characteristics
Temperature	Strong seasonal variation. The highest temperatures occur in the early summer months (June: 30.75 °C and July: 30.51 °C). The lowest temperatures are found in the winter (January: 10.55 °C). This indicates a large annual temperature range of approximately 20 °C
Relative humidity (RH)	Inversely correlated with temperature. The highest RH values occur in the cool winter months (January: 45.91% and February: 44.11%). The lowest RH is observed in the late spring/early summer (May: 26.04%), coinciding with the pre-monsoon hot and dry period
Wind speed (WS)	Peaks during the summer monsoon. The strongest winds are recorded from July (5.83 m s^{-1}) to August (5.59 m s^{-1}). The calmest wind conditions occur in the post-monsoon period (October: 3.47 m s^{-1} and November: 3.32 m s^{-1})

geopolitical hazards. Critical problems include the management of water resources, agricultural sustainability, pressures of urbanization, and hazards caused by the climate, such as flooding and droughts. It is important to gain a regional understanding of Pakistan when formulating policies and sustainable development initiatives.

The data from Fig. 2 in this study allow us to reconstruct the annual cycle.

Fig. 2 illustrates the research area's fundamental climate characteristics. Meteorological parameters, like relative humidity (RH), temperature (Temp), precipitation (pre), and wind speed (WS), are obtained from the AIRS satellite. The meteorological parameters over Pakistan indicate the highest temperature in June (30.75 °C) and July (30.51 °C), with the lowest temperature found in January (10.55 °C).

High precipitation values were noted in January (7.43 mm), June (7.68 mm), and December (6.34 mm), while the lowest precipitation was found in September (0.08 mm). Likewise, the highest RH (%) was found in January (45.91%) to February (44.11%), and the lowest one was recorded in May (26.04%). Similarly, the maximum wind speed was recorded from July (5.83 m s^{-1}) to August (5.59 m s^{-1}), and the minimum from October (3.47 m s^{-1}) to November (3.32 m s^{-1}).

Data sets

Atmospheric infrared sounder. Atmospheric Infrared Sounder (AIRS) is one of six instruments aboard NASA's Aqua spacecraft, which is part of NASA's Earth Observing System constellation of satellites.[19] AIRS provides global coverage twice a day, with 2378 spectral channels in the range of 0.41–15.4 μm. It travels over the equator at around 1:30 a.m. and 1:30 p.m. The AIRS instrument helps in a better understanding of the weather and climate on Earth. AIRS is a facility device designed to help conduct climate research and improve weather forecasting. Every day, NASA's Aqua satellite's atmospheric infrared sounder collects infrared light radiated from Earth's surface and atmosphere around the world. Its data include 3D temperature and water vapor readings throughout the atmosphere, as well as a variety of trace gases, surfaces, and cloud features. Weather prediction centers throughout the world use AIRS data to improve their forecasts. They are also used to test the accuracy of climate models and in a variety of applications, from detecting volcanic plumes to forecasting droughts. AIRS can also detect ozone, carbon monoxide, carbon dioxide, and methane, which are all trace GHGs. In contrast to MOPITT and certain other instruments, AIRS/AMSU retrieve methods offer cloud clearing for up to 80% cloud clearance. The significance of utilizing AIRS is that it can provide trace gases even during cloudy conditions without the use of information from the models. Thus, the present study has no missing data for the entire study duration. AIRS was put into orbit on May 4, 2002, by NASA's Aqua satellite. For this study, the monthly CO_2, CH_4, temperature, and relative humidity are used from 2002 to 2017 over Pakistan, obtained from AIRS (Giovanni), with spatial resolutions of 2.5° × 2° and 1° × 1°. The mid-troposphere is defined as a layer of atmosphere over the altitude range of 6–10 km (between approximately 500 and 300 hPa).[20] AIRS provides CO_2 data up to 2017, which is why we have carried out a study up to 2017. AIRS does not provide CO_2 data from 2002 to 2017 under one product, which is why we have taken monthly data of CO_2 from 2002 to 2012 from the product AIRX3C2MV005 and then taken CO_2 monthly data from 2013 to 2017 from another product, AIRS3C2MV005. The monthly variables like CO_2, CH_4 (mid-tropospheric) temperature, and relative humidity were taken from AIRS and averaged to create long-term annual averages. The data version/level of the Atmospheric Infrared Sounder used for CO_2 is AIRX3C2MV005, as well as AIRS3C2MV005, with a spatial resolution of 2.5° × 2°, and for CH_4, the level used is AIRS3STMV006, with a spatial resolution of 1° × 1°. AIRS CO_2 and CH_4 level 3 products used in the present study are sensitive to only the upper troposphere (mid to free troposphere).

Moderate resolution imaging radio spectrometer. The instrument known as the Moderate Resolution Imaging Spectroradiometer (MODIS) is currently operational on both Terra and Aqua satellites. With MODIS's 2330 km swath, it is feasible to view the world's data in a single day. MODIS algorithms have been upgraded periodically to enhance data quality and accuracy. The implementation of the Deep-Blue algorithm has enhanced MODIS Level 2 observations on bright surfaces, such as the Sahara Desert. Water vapor was measured in the current investigation using TERRA-MODIS (MODO5) level 2.0

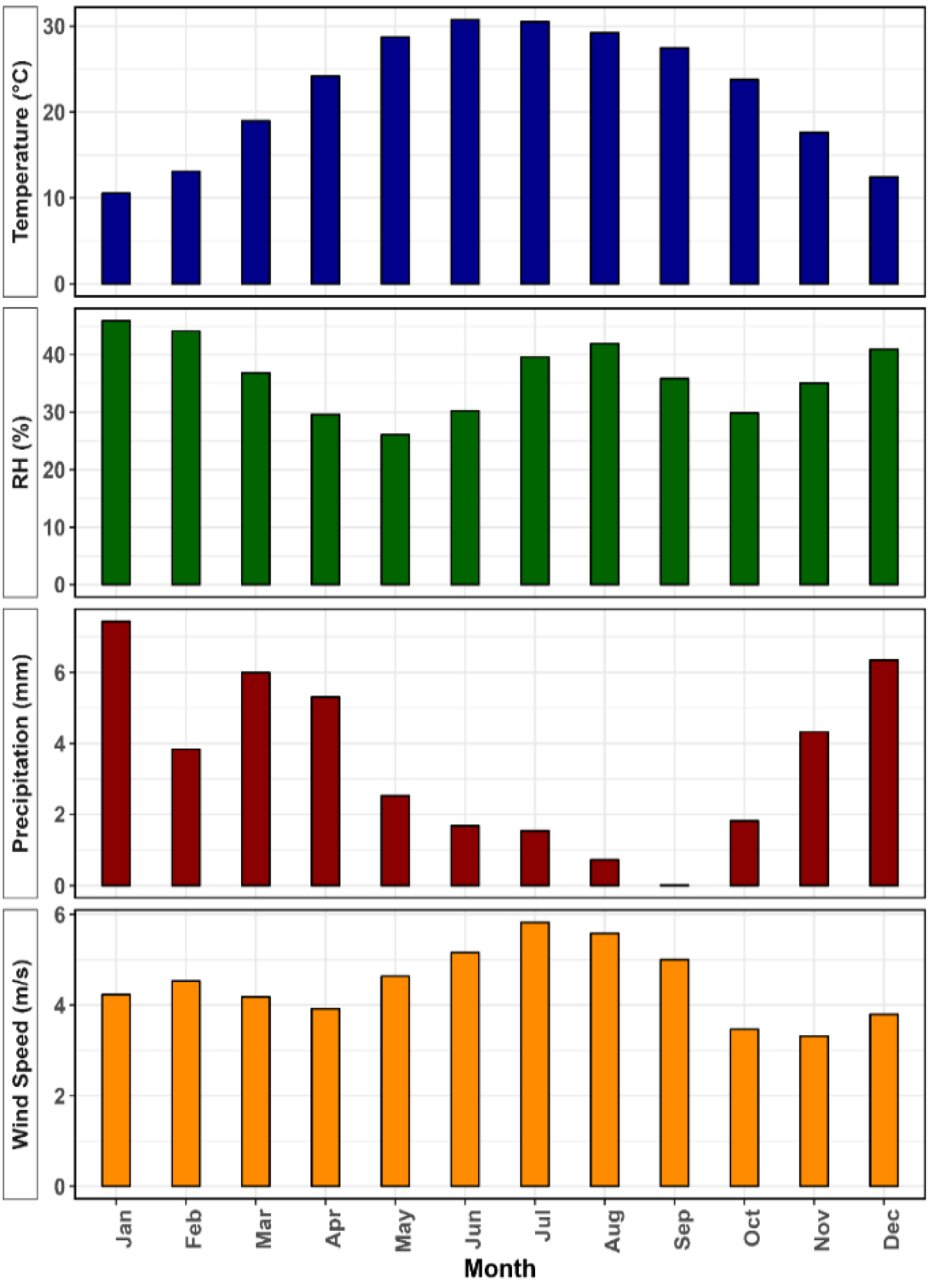

Fig. 2 Average monthly variations in meteorological parameters (including relative humidity, temperature, precipitation, and wind speed) over Pakistan during the study period (2002–2017).

collections of six products with a 1 × 1 km spatial resolution. The data of Cloud Fraction (CF) and Cloud Top Temperature (CTT) have been obtained from MODIS Satellite level MYD08M3V6.1, with a resolution of 1° × 1°. Monthly variables like NDVI, CF, and CTT were averaged to create a long-term annual average over the entire study location.

Additionally, we employed the 0.5° spatial resolution Normalized Difference Vegetation Index (NDVI) from the MODIS-Terra platform. NDVI is the ratio of albedo (α) measured at various wavelengths:

$$\mathrm{NDVI} = \frac{\alpha 0.86\ \mu\mathrm{m} + \alpha 0.67\ \mu\mathrm{m}}{\alpha 0.86\ \mu\mathrm{m} - \alpha 0.67\ \mu\mathrm{m}}. \quad (1)$$

In eqn (1), numerical values like 0.86 μm are used for NIR and 0.67 μm are used for red. NDVI values can vary from 0.1 to 1.0 despite their typical values being between 0.1 and 0.7. The higher values of NDVI symbolize increased canopy density and greenness[21,22]

Purpose of using MODIS cloud parameters. The authors used MODIS data for two key cloud parameters:

• Cloud Fraction (CF): The percentage of an area covered by clouds.

• Cloud Top Temperature (CTT): The temperature at the top of the clouds.

The purpose of including these parameters was to move beyond simply measuring gas concentrations and to start quantifying their climatic effects over Pakistan. Clouds play a critical role in the Earth's energy balance:

- They reflect incoming solar radiation (a cooling effect).
- They trap outgoing longwave (thermal) radiation (a warming effect).

By correlating GHG concentrations with cloud properties, the authors aimed to investigate if and how increasing levels of CO_2 and CH_4 are influencing local cloud characteristics, which in turn affect regional climate.

Modern-era retrospective analysis for the research and application model. Modern-Era Retrospective Analysis for Research and Applications-Model (MERRA) data, version 2, available since 1980, were used for the first comprehensive worldwide study of atmospheric aerosols and their interactions with other physical processes occurring in the climate system. Because of its ability to incorporate modern hyperspectral radiance and micro measurements, the MERRA-2 model represents an improvement over the original MERRA dataset and allows for developments in the assimilation mechanism. Additionally, this model uses ozone observations made by NASA since 2004. Weather and aerosol observations are modified for the MERRA-2 model using the Goddard Earth Observing System version 5 (GEOS-5). This model has a spatial resolution of 50 km in the latitudinal direction. The authors likely chose MERRA-2 because it is a global, long-term, and consistent reanalysis dataset specifically designed for atmospheric composition studies. Unlike operational models like ECMWF, MERRA-2 assimilates aerosol and chemical observations, providing meteorological data that is physically consistent with aerosol fields, which is crucial for studying pollutant interactions. It offers a complete spatial and temporal record that matches well with satellite overpasses. Precipitation and wind speed were measured in the current investigation using the MERRA-2 model (M2T1NXRAD) version 5.12.4 at a spatial resolution of $0.5° \times 0.625°$. The monthly variables, like precipitation and wind speed, were averaged to create long-term annual averages over the entire study location.

Methods

Trend analysis. During the study period, linear regression analysis was used to assess seasonal fluctuations. Nevertheless, sudden changes in the time series were not detectable using linear regression. To find these variations in the CO_2 and CH_4 concentrations, the study also used the Mann–Kendall (MK) sequential test.[23,24] The trend's significance was determined using the MK trend test statistic (Z) derived using the following formula:

$$z = \begin{cases} \dfrac{t-1}{\sqrt{\mathrm{var}(t)}}, & \text{if } t > 0 \\ 0, & \text{if } t = 0 \\ \dfrac{t+1}{\sqrt{\mathrm{var}(t)}}, & \text{if } t < 0 \end{cases}. \quad (2)$$

The probability of this normalized test statistic is calculated. The following equation gives the probability density function for a normal distribution with a mean of zero and a standard deviation of one:

$$p = \frac{1}{\sqrt{2\pi}} e^{\frac{z^2}{2}}. \quad (3)$$

- Decide on the degree of significance (95% is typical).
- A trend is said to be decreasing if Z is negative and the computed probability is greater than the level of significance. A trend is said to increase if Z is positive, and the computed probability is greater than the level of significance. There is no trend if the calculated probability is less than the level of significance.

$$U(t) = \frac{t - E(t)}{\sqrt{\mathrm{Var}(t)}}. \quad (4)$$

The sequential numbers $U(t)$ and $U'(t)$ from the Mann–Kendall test's progressive analysis were calculated to observe how the trend changed over time.[25] $U(t)$ is the sum of the z values found from the first to the last data point. This test considers the relative values of all terms in the time series (x_1, x_2,…, x_n). The following steps are sequentially applied. The magnitudes of the x_j annual mean time series ($j = 1, 2, \ldots, n$) are compared with x_i ($I = 1, 2, \ldots, j-1$). For each comparison, the number of cases $x_j > x_i$ is counted and denoted by n_j.

- The test statistic t is thus provided using the following equation:

$$t = \sum_{i=1}^{n} n_i. \quad (5)$$

- Mean and variance of the test statistic are respectively

$$E(t) = \frac{n(n-1)}{4} \quad (6)$$

$$\mathrm{Var}(t) = \frac{n(n-1)(2n+5)}{72}. \quad (7)$$

- We can calculate the sequential values of the statistic $U(t)$ using the following equation:

$$U(t) = \frac{t - E(t)}{\sqrt{\mathrm{Var}(t)}}. \quad (8)$$

Similarly, $U'(t)$ values are computed backward, starting at the end of the series. The sequential Mann–Kendall model could be regarded as an effective method for determining the beginning year(s) of a trend. If the values are greater than the confidence interval (1.96), the hypothesis of no change is rejected, and the approximate time of the change point (abrupt change) is shown by the intersection of and $U'(t)$ in the time series.

Hybrid single-particle Lagrangian integrated Trajectory model. The study used the Hybrid Single-Particle Lagrangian

Integrated Trajectory (HYSPLIT) model to examine air mass paths in the study domain to comprehend the role of long-distance sources of pollution. A 5 days backward air mass trajectory over the study region with an altitude between 500 m and 10 000 m above ground level was considered. The HYSPLIT model-based Trajstat software was used to calculate all air mass trajectories.[26]

Results and discussion

Monthly and seasonal variations in the concentration of CO_2

The variation in the concentration of CO_2 observed from the satellite AIRS during the study period (2002–2017) is shown in Fig. 3(a) and (b). The annual cycle of CO_2 shows a gradual increase from November to May and then decreases up to October. The findings revealed that the CO_2 concentration reached a maximum value in May and then sharply declined after June, with October recording the lowest levels. During the study period (2002–2017), the average CO_2 levels ranged from 376 to 404, with an average value of (389 ± 8) ppmv in May, while they ranged from 371 to 402, with an average (386 ± 8) ppmv in October. Average seasonal CO_2 concentrations were found to be high during spring and low during autumn (Fig. 3b). Since lower temperatures and solar radiation during the autumn (dry season) prevent increases in local CO_2 assimilation, the lowest CO_2 at this time may be caused by respiratory carbon loss.[27] As the season changed from winter to pre-monsoon months, a consistent rise in CO_2 concentration was noted. Spring is enhanced because of the higher temperatures and more sunlight that occur during these months, which promotes respiration at night and CO_2 assimilation during the day.[28] The increased CO_2 concentration during these months is complemented by improved soil respiration. The spring CO_2 concentration in the Indian subcontinent can also be significantly impacted by biomass burning in addition to these natural factors. The monsoon months observe the lowest CO_2 levels primarily due to increased photosynthetic processes introduced by more soil moisture. As the monsoon progresses, a reduction in CO_2 concentration is also noted. Because of the dark and cloudy weather that prevails throughout these months, the temperature drops, which lowers soil and leaf respiration and increases carbon uptake.[29] High ecosystem productivity and increased microbial activity are linked to further increases in CO_2 during the autumn season.[12]

Because there is insufficient quality control by the relevant authorities, CO_2 concentration may be a byproduct of burning low-grade fuel and using an inappropriate combustion system, which can be found on the open market. The main sources of CO_2 concentration in the study locations included traffic congestion, road conditions, and industrial exhaust, and related results were apparent from Ul Haq *et al.*[30] in Pakistan. Kuttippurath *et al.*[31] found the highest CO_2 concentration in India during the spring season during their study period (2002–2020). Coa *et al.*[32] found the highest CO_2 concentration in spring (384.0 ppm) and the lowest in winter (382.5 ppm) over six locations globally from 2003 to 2011. Wei *et al.*[33] found that the

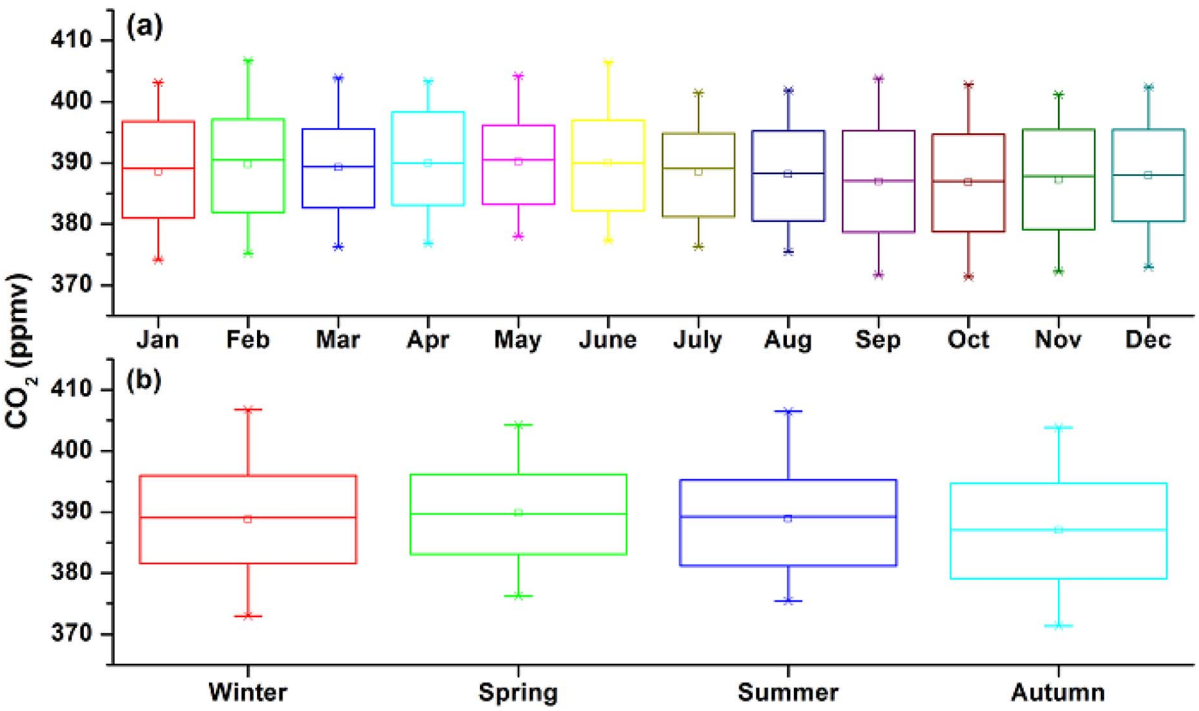

Fig. 3 Summary of Box–Whisker plots: (a) monthly variations in CO_2 and (b) seasonal variations in CO_2 over the entire region. Each box indicates the 25th and 75th percentiles and the whiskers show the 5th and 95th percentiles. The vertical lines show the standard deviation from the mean value. The solid circle inside each box and the horizontal lines represent the mean and median values, respectively. The crosses above and below the boxes indicate the maximum and minimum values, respectively. Seasons are categorized as winter (December, January, and February), spring (March, April, and May), summer (June, July, and August), and autumn (September, October, and November).

average concentrations of CO_2 were 428.36 ± 13.96 ppm in the megacity of Shanghai, China, from 2017 to 2018, with the highest CO_2 concentration in winter and the lowest in autumn. Kumar *et al.*[34] also investigated the highest values of CO_2 during the spring season in India. Metya *et al.*[35] found an average CO_2 concentration of 406.05 ± 6.36 ppm at Sinhagad, India, and attains its minimum concentration during autumn, whereas CO_2 reaches its maximum concentration during spring.

The key reasons for the nature of the CO_2 cycle are as follows:

1. Lag in photosynthesis: in spring, warmer temperatures cause a rapid increase in soil and plant respiration (a CO_2 source), but the full photosynthetic drawdown (the CO_2 sink) from vegetation has not yet reached its peak. This temporary imbalance causes CO_2 to accumulate, leading to a peak in May.

2. Biomass burning: specifically in the Indian subcontinent, widespread agricultural and forest fires in the pre-monsoon (spring) season add a significant pulse of CO_2 to the atmosphere, reinforcing the natural peak.

In winter, respiration is lower due to cold temperatures. Although human emissions from heating are high, the lack of this large biogenic CO_2 release from soils means that the concentration does not reach the levels observed in the spring.

Monthly and seasonal variations in the concentration of CH_4

CH_4 had the maximum value in August and reached its lowest level in April. In August, the concentration of CH_4 ranged from 1860 ppbv (lowest value) to 1891 ppbv (highest value), with an average of 1876 ± 10 ppbv. In contrast, in April, CH_4 varied from 1784 to 1855 ppbv, with an average of 1820 ± 21 ppbv. CH_4 concentration was noted to have a maximum value during summer and a low value during the spring season (Fig. 4b).

In the troposphere, the balance between surface emission and OH destruction mostly determines the concentration of CH_4. In the Indian subcontinent, ruminants, rice paddies, and wetlands are the main sources of CH_4.[36] The Kharif (monsoon) season may be linked to the maximum concentration, which occurs during the summer.[37] The seasonality of the CH_4 concentration over Asia is characterized by greater values in the wet season and lower values in the dry season.[38] This could be because of strong emissions from wetlands and rice fields during the wet season. During the winter and spring seasons, low mixing ratios of CH_4 were primarily caused by a decrease in atmospheric hydrocarbons because of fewer photochemical reactions and a significant drop in solar intensity.[39] The summer and autumn seasons showed a significant rate of CH_4 change. According to Nishanth *et al.*[40] and Goroshi *et al.*,[37] the interchange of CH_4 between rice paddy fields and the atmosphere is governed by both biological and physical processes. This is why in the current study area, more CH_4 is observed during the summer and autumn seasons.

Kavitha and Nair[41] found the maximum CH_4 concentration during August/September over various locations in India from 2003 to 2009 and investigated the CH_4 concentration that ranged from the minimum value of 1740 ppm to the maximum value of 1890 ppm using satellite data. They also observed the peak value of CH_4 concentration during the monsoon and post-monsoon seasons and the minimum during the winter season. They associate CH_4 concentration with livestock distribution

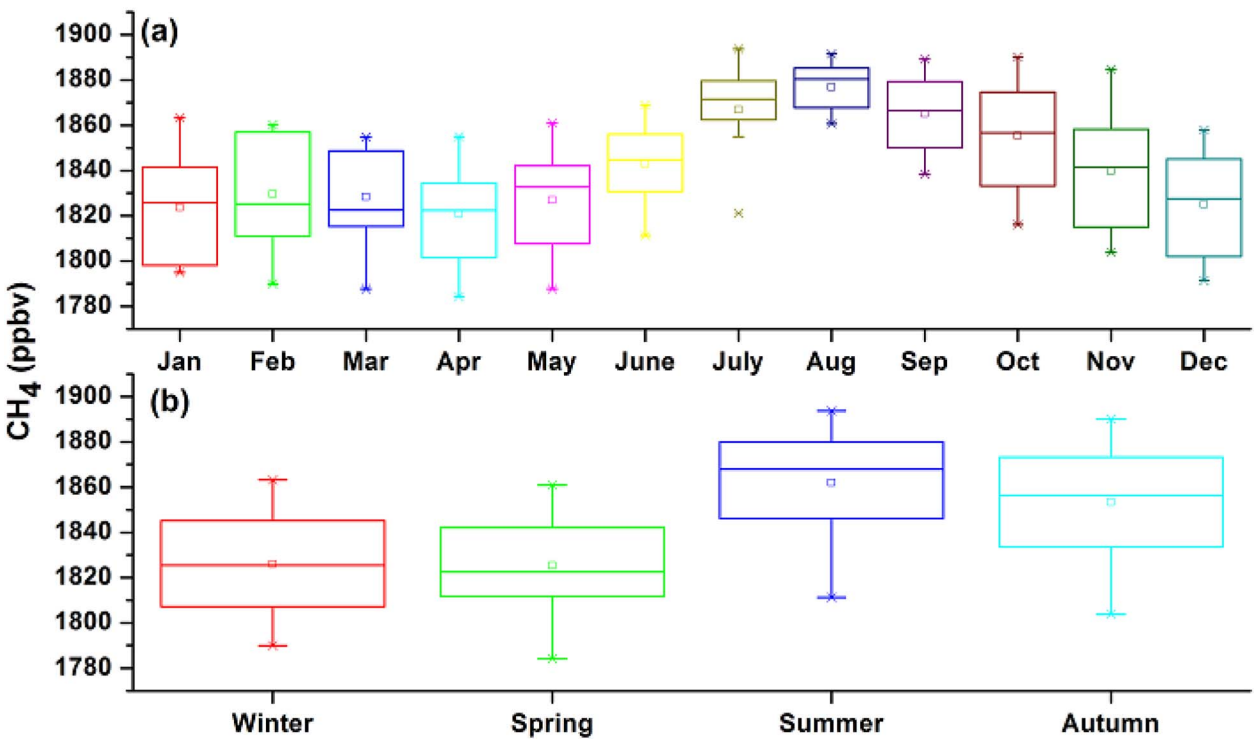

Fig. 4 Box–Whisker plots indicating (a) monthly variations in CH_4 and (b) seasonal variations in CH_4 over Pakistan. The Box–Whisker representation in all panels is the same as in Fig. 3.

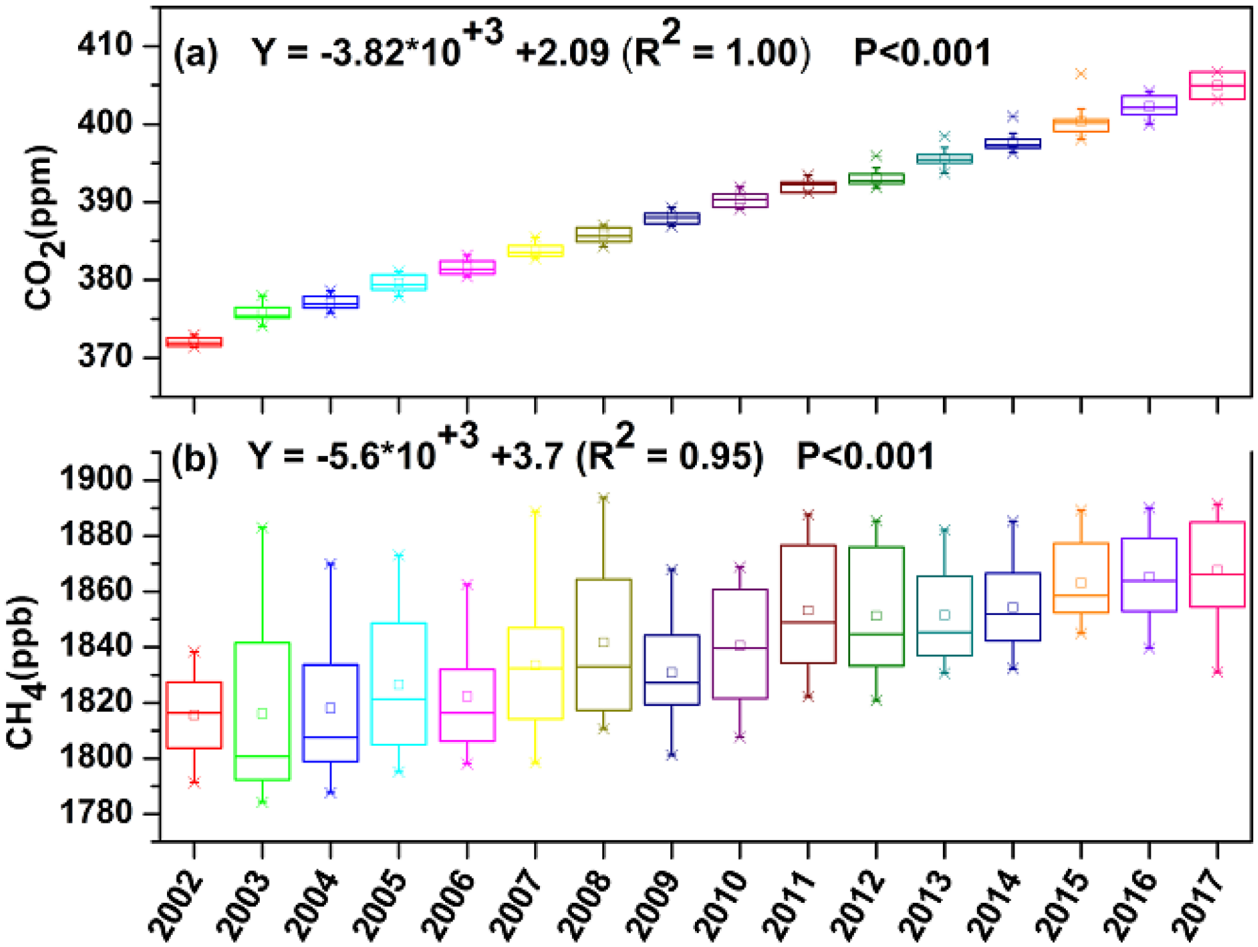

Fig. 5 Box–Whisker plots indicate an inter-annual variation in (a) CO_2 and (b) CH_4 over Pakistan from 2002 to 2017. The Box–Whisker representation in all panels is the same as that depicted in Fig. 4.

and wetland emission, including rice fields. Ul Haq *et al.*[30] observed the maximum concentration of CH_4 during summer (1804 ± 28) ppb, followed by autumn (1800 ± 25 ppb) and winter (1777 ± 24 ppb) over Pakistan, Afghanistan, and adjoining areas using satellite data from 2003 to 2012. Wei *et al.*[33] reported the average concentrations of CH_4 to be 2154 ± 190 ppb, in the megacity of Shanghai, China, from 2017 to 2018, with the highest value in summer and the lowest one in spring.

Inter-annual patterns

The long-term trends from 2002 to 2017 (Fig. 5a and b) reveal a significant and consistent increase in tropospheric CO_2 and CH_4 concentrations over Pakistan. Linear regression analysis quantified the annual growth rates at 2.1 ppm per year for CO_2 and 3.5 ppb per year for CH_4 (Table 2). Both trends were highly statistically significant ($p \leq 0.05$), with coefficients of determination (R^2) exceeding 0.95, confirming a remarkably steady and robust upward trajectory. This cumulative growth resulted in an overall increase of 8.6% for CO_2 (*e.g.*, from ~376 ppm to ~406 ppm) and 2.9% for CH_4 over the 16 years. By 2017, seasonal peaks had risen to values exceeding 406 ppm for CO_2 (in May) and 1867 ppb for CH_4 (in August). This sharp rise is unequivocally attributed to anthropogenic emissions from fossil fuel combustion, industrial activity, agriculture, and biomass burning, surpassing the capacity of natural sinks, a situation exacerbated by extensive deforestation.

The observed trend for CO_2 (2.1 ppm per year) aligns closely with findings from regional and global studies. Kuttippurath *et al.*[31] reported an average trend of ~2.1 ppm per year over India, while Cao *et al.*[32] found a nearly identical global mid-

Table 2 Statistical metrics of the long-term linear trends (2002–2017) for CO_2 and CH_4 over Pakistan

Greenhouse gas	Trend	Slope (change per year)	R^2 (coefficient of determination)	P-value	Overall increase (2002–2017)
CO_2	Significant increase	+2.1 ppm per year	>0.95 (very high)	$P \leq 0.05$	8.6% (*e.g.*, ~376 to ~406 ppm)
CH_4	Significant increase	+3.5 ppb per year	>0.95 (very high)	$P \leq 0.05$	2.9% (*e.g.*, ~1791 to ~1858 ppb)

Table 3 Variations (seasonal) in the concentration of CO_2 (ppm) and CH_4 (ppm) over Pakistan from 2002 to 2017

Year	Winter season	Spring season	Summer season	Autumn season
Average conc. Of CO_2(ppm)				
2002	372	376	375	371
2003	375	377	376	375
2004	376	380	377	376
2005	378	383	379	378
2006	381	383	381	380
2007	382	385	383	383
2008	384	386	385	384
2009	386	388	387	387
2010	389	391	390	389
2011	392	393	392	391
2012	392	393	392	392
2013	394	396	395	395
2014	397	397	398	396
2015	399	401	402	399
2016	401	403	400	400
2017	403	403	400	401
Average conc. Of CH_4(ppb)				
2002	1791	1780	1862	1823
2003	1794	1788	1852	1828
2004	1801	1796	1849	1824
2005	1807	1845	1854	1836
2006	1802	1810	1839	1834
2007	1809	1817	1866	1839
2008	1817	1822	1875	1850
2009	1820	1817	1843	1840
2010	1825	1816	1858	1859
2011	1830	1839	1868	1872
2012	1831	1831	1869	1873
2013	1845	1838	1871	1865
2014	1849	1839	1862	1864
2015	1852	1852	1875	1871
2016	1855	1844	1875	1884
2017	1858	1846	1878	1885

tropospheric increase of 2.11 ppm per year. Similarly, the CH_4 growth rate of 3.5 ppb per year is consistent with the significant increases documented in South Asia. For instance, Mahmood *et al.*[15] reported a rise of 5.02 ppb per year over Pakistan from 2003 to 2015. The findings of Ul Haq *et al.*,[30] who observed a 3.7% increase in CH_4 over a decade, further corroborate the persistent and widespread nature of increasing GHG concentrations across the region; these rates are primarily driven by anthropogenic activities rather than natural variability.

The seasonal variation in the concentration of both CO_2 and CH_4 in Table 3 shows that CO_2 has a relatively high value of 403 ppm during the spring season. Likewise, CH_4 shows maximum values (1885 ppb) during the autumn season. It is determined that $P \leq 0.05$ denotes a considerable rise in the concentration of both gases.

Interpretation of Mann–Kendall (MK) and sequential Mann–Kendall (SQMK) tests

Abrupt changes in GHG trends: insights from Mann–Kendall analysis. The application of the Sequential Mann–Kendall (SQMK) test (Fig. 6, 7, and 9) provides a more nuanced understanding of the trends, revealing specific years when significant abrupt changes (change-points) began in the concentrations of CO_2 and CH_4 over Pakistan.

Interpreting the SQMK test. The forward sequential statistic ($U(t)$) represents the progressive analysis of the time series from start to end. The backward statistic ($U'(t)$) is calculated from the end to the start. A change-point year is identified where these two statistics intersect (cross) and diverge beyond the confidence limits (typically ± 1.96 for 95% significance). This intersection signifies the initiation of a statistically significant shift in the trend's magnitude or direction.

Identified change-points and interpretation. • CO_2 abrupt change (Fig. 6 and 9b): The SQMK analysis for CO_2 indicates a major, sustained change-point starting around 2009. This is evidenced by the clear and persistent divergence of $U(t)$ and $U'(t)$ beyond the confidence limits after this year across all seasons (Fig. 6a–d) and in the annual data (Fig. 9b). The remarkable consistency of this change-point across all seasons suggests a large-scale, systemic driver that affected CO_2 emissions or sinks throughout the entire year, overriding seasonal variations. These points strongly to a significant intensification of anthropogenic activities, such as a rapid increase in fossil fuel consumption, industrial output, or energy production within

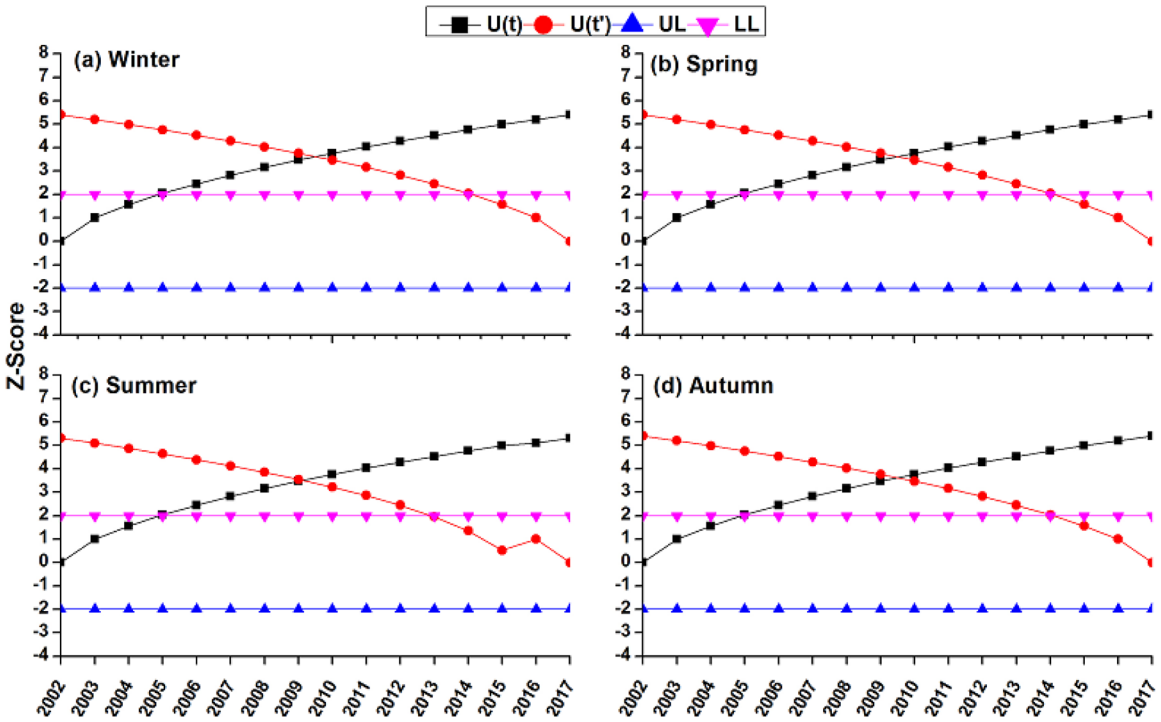

Fig. 6 An abrupt change in CO_2 resulting from the sequential Mann–Kendal test statistics during (a) winter, (b) spring, (c) summer, and (d) autumn. U(t) is known as the forward sequence, which follows a normal distribution. U′(t) is denoted as the backward sequence derived from eqn (8), and UL and LL denote the upper and lower limits. The significance of the trend was calculated using the MK trend test statistic (Z) from eqn (2). Generally, $Z > 0$ indicates an increasing trend, $Z < 0$ indicates a decreasing trend, and $Z = 0$ indicates no trend.

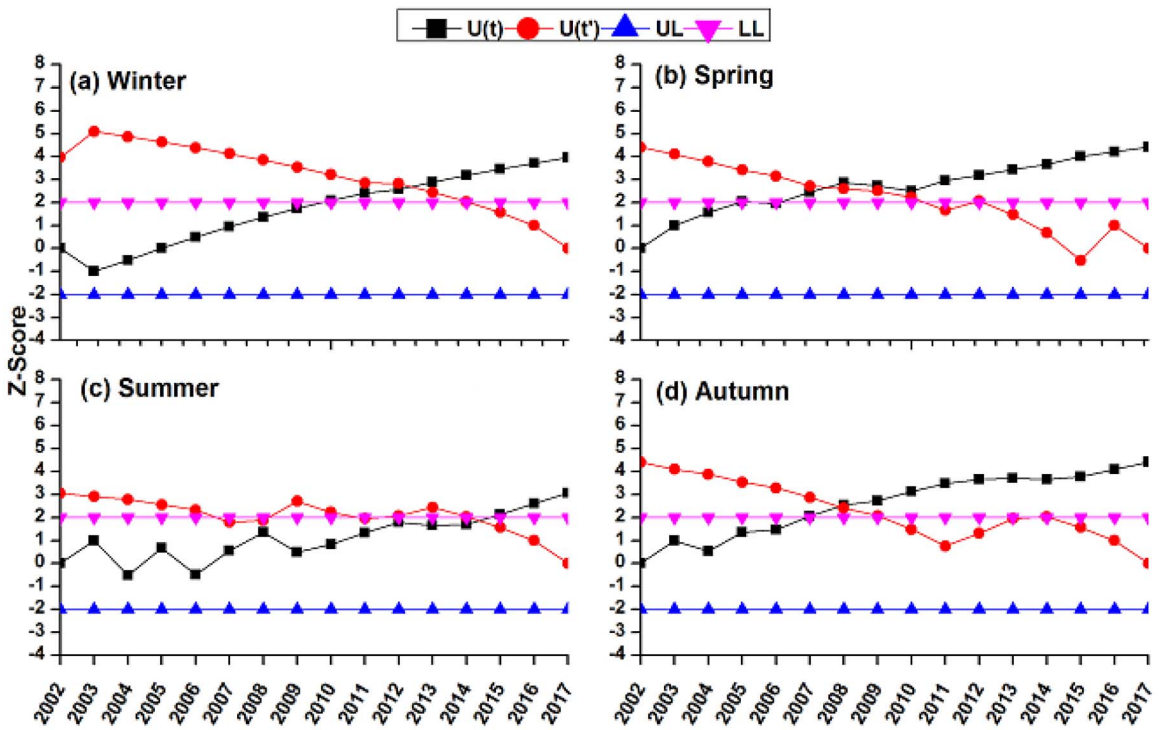

Fig. 7 An abrupt change in CH_4 resulting from the sequential Mann–Kendal test statistics during (a) winter, (b) spring, (c) summer, and (d) autumn. The various terms like $U(t)$, $U'(t)$, UL, LL, and Z have the same representation, as shown in Fig. 6.

the region, likely linked to economic recovery and growth patterns in South Asia post-2008.

• CH_4 Abrupt Changes (Fig. 7 and 9c): The change-points for CH_4 are more complex and variable than for CO_2. The annual analysis (Fig. 9c) suggests a potential shift beginning around 2010–2011, with U(t) crossing the confidence limit. However, the seasonal analysis (Fig. 7a–d) reveals a more scattered pattern, with intersections and divergences occurring at different times (*e.g.*, ~2008 in autumn and ~2012 in winter). This scattered nature suggests that the drivers for methane are more complex and season-specific, which is likely influenced by a combination of anthropogenic activity and climatic variables. For instance, change-points in spring/autumn could be linked to modifications in agricultural practices (*e.g.*, rice cultivation patterns and livestock management), while those in winter/summer may be related to shifts in monsoon patterns or temperature, which control microbial methane production in wetlands and rice paddies.

• Temperature trend shift (Fig. 9a): the SQMK test for temperature reveals a highly significant change-point starting around 2009, with $U(t)$ sharply and permanently exceeding the upper confidence limit. This timing coincides precisely with the change-point identified for CO_2. This synchronicity suggests a potential climate feedback mechanism, where the continued accumulation of CO_2 and other GHGs began to manifest a more pronounced and consistent warming signal in the regional climate system from that year onward.

Correlation of CO_2 with NDVI, CF, CTT, and other meteorological parameters

The correlation analysis reveals the complex interplay between CO_2 concentrations and environmental drivers over Pakistan (Fig. 8 and Table 4). The key findings and their logical interpretations are.

CO_2 and NDVI ($r = -0.50$ and $p = 0.01$)

The significant negative correlation robustly confirms the role of vegetation as a carbon sink. Higher NDVI values, indicating greater photosynthetic activity (particularly during the monsoon and post-monsoon seasons), correspond with lower atmospheric CO_2 levels due to active carbon uptake. Conversely,

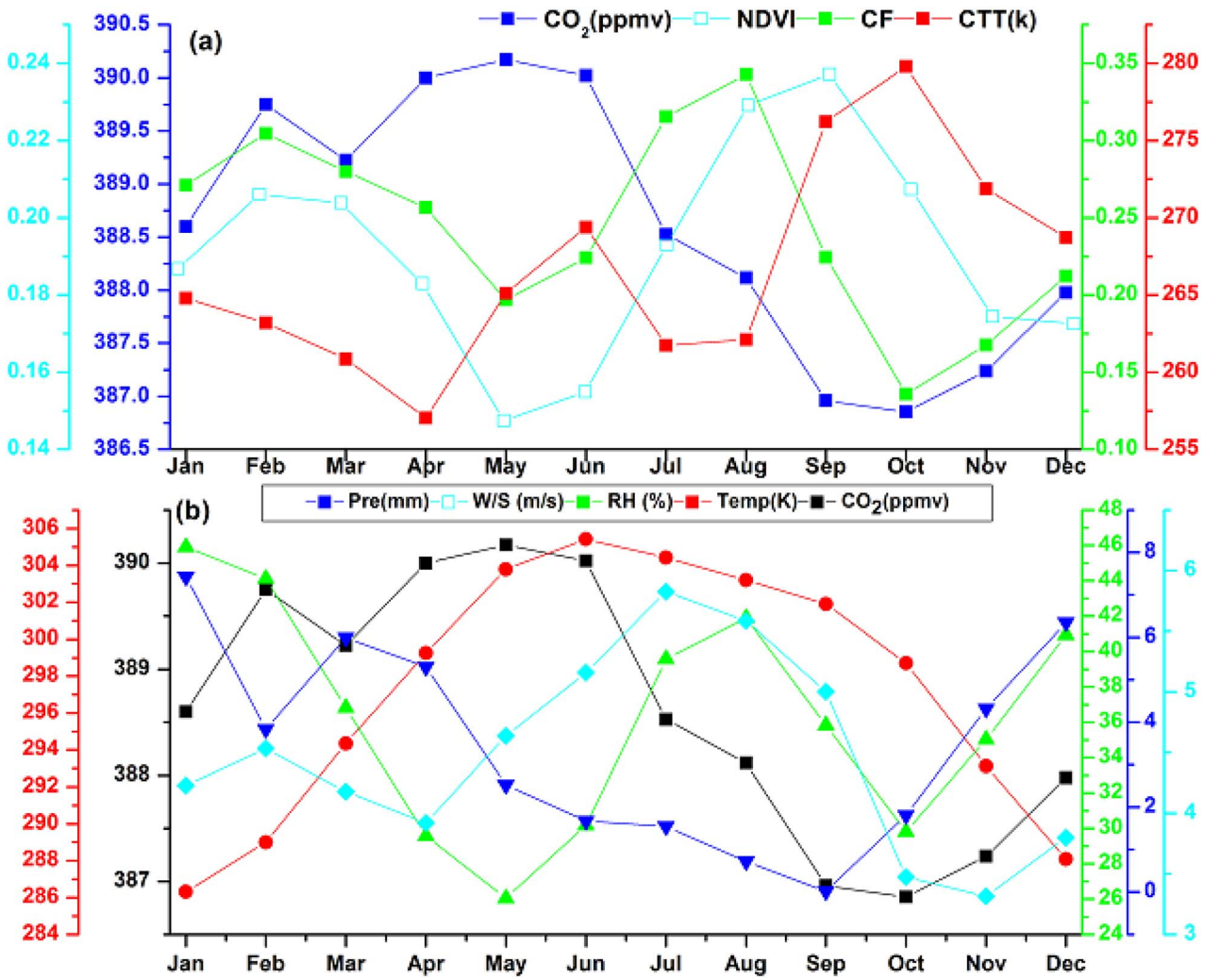

Fig. 8 Average monthly variations in the concentrations of (a) CO_2 *vs.* NDVI, CF, and CTT, and (b) CO_2 *vs.* Temp, RH, Pre (precipitation), and W/S (wind speed).

Table 4 Correlation coefficients (r) of CO_2 and CH_4 with CF, CTT, Temp, RH, Pre, and WS

CO_2 and NDVI	CO_2 and CF	CO_2 and CTT	CO_2 and Temp	CO_2 and RH	CO_2 and Pre	CO_2 and wind speed
−0.50 $P = 0.01$	−0.36 $P = 0.02$	0.31 $P = 0.03$	0.12 $P = 0.001$	−0.45 $P = 0.003$	−0.23 $P = 0.05$	−0.35 $P = 0.08$
CH_4 and NDVI	CH_4 and CF	CH_4 and CTT	CH_4 and Temp	CH_4 and RH	CH_4 and Pre	CH_4 and wind speed
0.64 $P = 0.001$	−0.20 $P = 0.009$	0.32 $P = 0.07$	0.60 $P = 0.06$	0.29 $P = 0.005$	−0.65 $P = 0.01$	0.61 $P = 0.04$

the CO_2 peak in spring occurs when respiration from soils and vegetation outpaces the regrowth of photosynthetic capacity and is exacerbated by widespread biomass burning.

CO_2 and meteorological parameters

Temperature ($r = 0.12$ and $p = 0.001$): the weak positive correlation suggests that higher temperatures enhance soil and plant respiration rates, releasing more CO_2. However, the weakness of the correlation indicates that local temperature is not the dominant driver, which is overshadowed by larger-scale anthropogenic emissions and photosynthetic drawdown.

Precipitation ($r = -0.23$ and $p = 0.05$) and relative humidity ($r = -0.45$ and $p = 0.003$): the negative correlations align with the seasonal cycle. The dry pre-monsoon season (low precipitation/RH) is associated with peak CO_2 from fires and respiration. The wet monsoon season (high precipitation/RH) corresponds with CO_2 drawdown due to enhanced photosynthesis and reduced fire activity.

Wind speed ($r = -0.35$ and $p = 0.08$): the negative relationship suggests that higher winds promote the dispersion and dilution of locally emitted CO_2, leading to lower observed concentrations, particularly in polluted boundary layers.

CO_2 and cloud properties (climatic response)

Cloud top temperature (CTT) ($r = 0.31$ and $p = 0.03$): the positive correlation is a critical indicator of greenhouse forcing. Increased CO_2 absorbs more longwave radiation, warming the atmospheric layer. This warming can lead to higher cloud top temperatures or a shift in cloud formation to lower, warmer altitudes, reinforcing the warming effect.

Cloud fraction (CF) ($r = -0.36$ and $p = 0.02$): the negative correlation is complex. It may reflect meteorological patterns where drier, high-pressure systems (favoring clear skies) coincide with stable conditions that allow CO_2 to accumulate. Conversely, cloudy conditions often accompany precipitation and vertical mixing that dilute CO_2.

In summary, CO_2 variability is primarily driven by a combination of biological activity (source and sink) and anthropogenic emissions, modulated by meteorological conditions that control dispersion and dilution. The correlations with cloud properties suggest that rising CO_2 interacts with and potentially modifies local cloud characteristics, contributing to regional climate feedbacks.

Pathakoti *et al.*[42] found correlation coefficients of 0.13, −0.18, −0.32, and −0.50 between CO_2 and Temp, WS, RH, and Prec, respectively, over Bharati (India) in 2016. Kumar *et al.*[34] found correlation coefficients of 0.8 and −0.64 between CO_2 and temperature and NDVI, respectively, over India from 2004 to 2011. Kumar *et al.*[34] also found a negative correlation between mid-tropospheric CO_2 and rainfall over India.

Sreenivas *et al.*[22] investigated that during pre-monsoon, monsoon, post-monsoon, and winter, the corresponding correlation coefficients (R_s) between wind speed and CO_2 are 0.56, 0.32, 0.06, and 0.67, respectively, over Shadnagar, a suburban site of Central India, in the year 2014. Nyasulu *et al.*[43] reported a significant association between temperature (T, °C) and CO_2 ($r = 0.75$ and $p < 0.01$) during the SON pollution peak season. Additionally, during SON, CO_2 had a substantial negative association with the cloud fraction ($r = -0.55$ and $p < 0.05$) and a significant positive correlation with cloud top temperature ($r = 0.56$ and $p < 0.05$). These findings suggest that trace gases have a considerable impact on the climate during periods of heavy pollution.

Metya *et al.*[35] found that correlation coefficients (R) between wind speed and CO_2 during monsoon, post-monsoon, winter, and pre-monsoon are 0.51, 0.15, − 0.02, and − 0.28, respectively. A good inverse correlation between GHG and wind speed suggests that with an increase in wind speeds, GHG concentrations decrease. In contrast, a weaker correlation suggests that regional/local transport plays some roles.[44] Strong winds, especially during the monsoon season, are likely to dilute GHG concentration. The changes in CO_2 and CH_4 concentrations are linked to the adjusted temperature, and it was found that both gases have been increasing from the beginning of the study period (2002), but temperature showed an increasing trend only after 2009. As is clear from Fig. 9a–c, comparing the temperature trends with those of trace gases indicates that both temperature and trace gases are increasing over the study area, and a steady increase in temperature from 2009 onwards coincides with the change point for CO_2.

Correlation of CH_4 with NDVI, CF, CTT, and other meteorological parameters

The correlation analysis for CH_4 reveals a distinct set of drivers compared to CO_2, which is heavily influenced by microbial processes and agricultural practices (Fig. 10 and Table 3).

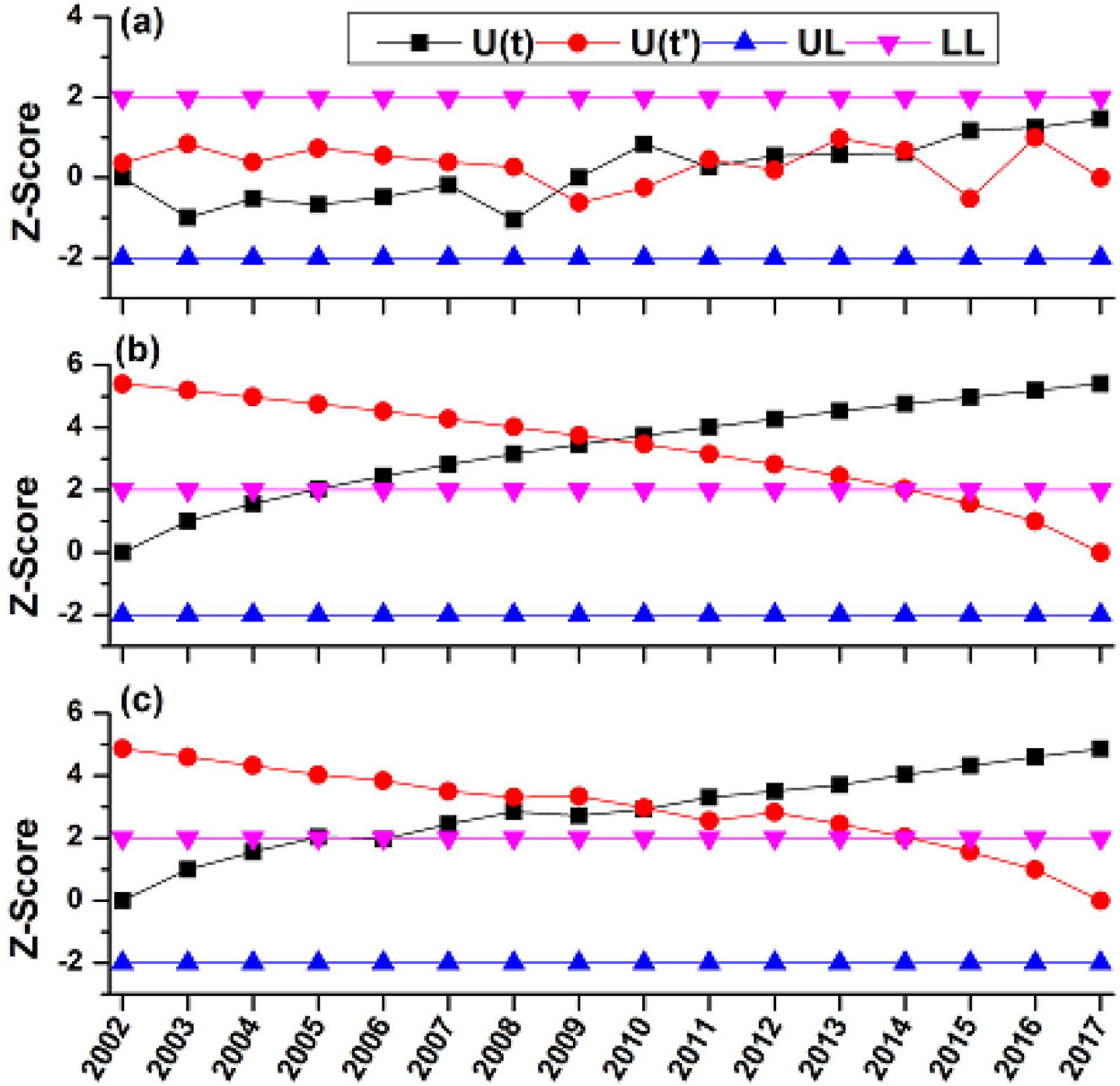

Fig. 9 Annual abrupt change in (a) temperature, (b) CO_2, and (c) CH_4 resulting from the sequential Mann–Kendal test statistics. The various terms like $U(t)$, $U'(t)$, UL, LL, and Z have the same representation as that depicted in Fig. 6.

CH_4 and NDVI ($r = 0.64$ and $p = 0.001$)

The strong positive correlation is counterintuitive at first glance but is a hallmark of agricultural methane sources. High NDVI over Pakistan is often linked to irrigated croplands, particularly rice paddies. Flooded fields create anaerobic conditions in which methanogenic archaea thrive, converting organic matter into CH_4. Thus, greener landscapes from agriculture can directly correlate with higher methane emission rates.

CH_4 and meteorological parameters

Temperature ($r = 0.60$ and $p = 0.06$): the strong positive correlation is a key control on microbial methane production. Warmer temperatures significantly increase the metabolic rates of methanogens in wetlands, rice fields, and soils, leading to higher emission rates, especially during the summer season.

Precipitation ($r = -0.65$ and $p = 0.01$): the strong negative correlation is likely indirect and related to atmospheric chemistry, not emissions. Higher precipitation is associated with increased cloud cover and reduced solar radiation, which lowers the atmospheric concentration of hydroxyl radicals (OH), the primary sink for methane. With its main removal mechanism weakened, CH_4 concentrations accumulate.

Wind speed ($r = -0.61$ and $p = 0.04$): similar to CO_2, the negative correlation indicates that higher wind speeds disperse and dilute concentrated plumes of CH_4 from point sources like wetlands, agricultural areas, and leaks from infrastructure.

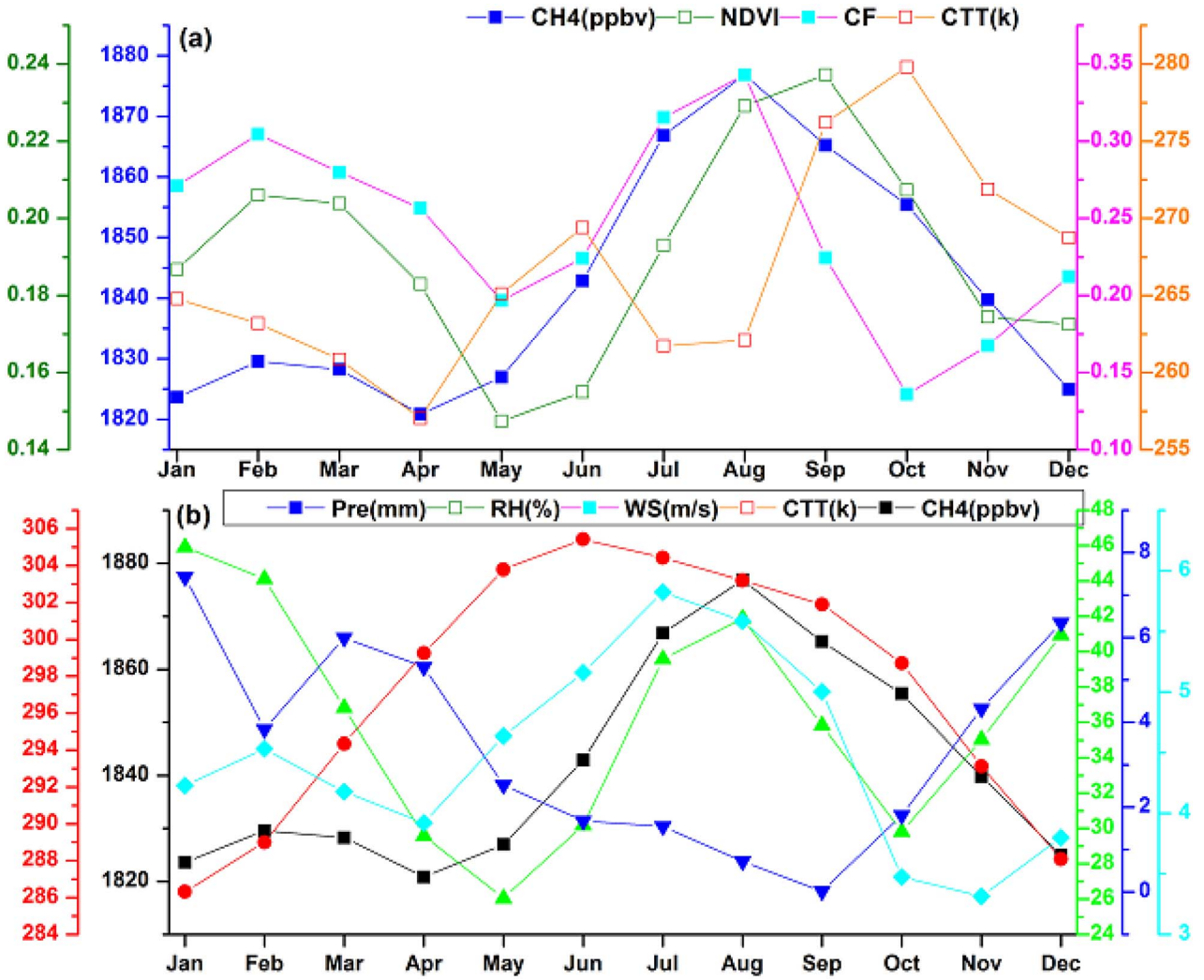

Fig. 10 Average monthly variations in the concentrations of (a) CH_4 *vs.* NDVI, CF, and CTT, (b) CH_4 *vs.* Pre, RH, WS, and Temp.

CH_4 and cloud properties (climatic response)

Cloud top temperature (CTT) ($r = 0.32$ and $p = 0.07$): as with CO_2, the positive trend suggests that CH_4 contributes to lower atmospheric warming, which may be reflected in warmer cloud tops, consistent with its role as a potent greenhouse gas.

Cloud fraction (CF) ($r = -0.20$ and $p = 0.03$): the weak negative correlation may again reflect synoptic weather patterns where conditions favouring CH_4 buildup (*e.g.*, low wind and stable atmosphere) may also be associated with fewer clouds.

In summary, CH_4 concentrations are predominantly driven by temperature-dependent microbial emissions from agriculture (rice) and natural wetlands, as evidenced by the strong link between NDVI and temperature. Its atmospheric lifetime is further modulated by meteorological factors that control its destruction (*via* OH), leading to an observed strong negative correlation with precipitation.

Khaliq *et al.*[10] showed that the CH_4 concentration was significantly affected by anthropogenic emissions, NDVI, meteorological parameters, and soil moisture over South, East, and Southeast Asia from 2009 to 2020. Sreenivas *et al.*[21] also reported a positive correlation between CH_4 and NDVI in a suburban site in India. Metya *et al.*[35] noted a positive correlation between CH_4 and NDVI over Sinhagad, located on the Western Ghats in peninsular India. Nyasulu *et al.*[43] also found a positive correlation between CH_4 and NDVI over Muzambiq, Africa.

Sreenivas *et al.*[21] found that pre-monsoon, monsoon, post-monsoon, and winter wind speed and CH_4 correlation coefficients (Rs) are 0.28, 0.71, 0.21, and 0.60, respectively, over Shadnagar, India, in 2014.

Nyasulu *et al.*[43] found that the autumn season is the pollution peak season and there is a significant association between temperature (T °C) and CH_4 ($r = 0.80$ and $p < 0.01$). In addition, during autumn, CH_4 demonstrated a strong negative association with cloud percentage ($r = -0.69$ and $p < 0.01$) and a large positive correlation with cloud top temperature ($r = 0.74$ and $p < 0.01$). These findings suggest that trace gases have a considerable impact on the climate.

According to Metya *et al.*,[35] the correlation coefficients (R) between wind speed and CH_4 are −0.57, −0.3, −0.02, and −0.2 in the monsoon, post-monsoon, winter, and pre-monsoon seasons, respectively. Conversely, a lower correlation implies

that local or regional emissions are important.[47] The GHG concentration is expected to be diluted by strong winds, particularly during the monsoon season. This is confirmed for CH_4, where there is a negative correlation between wind and CH_4 concentration ($R = -0.61$).

The changes in CO_2 and CH_4 concentrations were tried to link to the adjusted temperature, and it was found that both gases showed an increasing trend from the beginning of the study period (2002), but temperature showed an increasing trend only after 2009. The observed temperature pattern indicates an increasing trend. As shown in Fig. 9a–c, comparing the temperature trends with those of trace gases indicates that both temperature and trace gases are increasing over the study area, and a steady increase in temperature from 2009 onwards coincides with the change point for CH_4. During the study period, a steady temperature rise signifies a temperature response to a significant increase in trace gases.

Essence of the observed correlations

The correlations found between the trace gases and cloud parameters are not necessarily about gases causing changes in clouds directly but rather about what these relationships reveal about the radiative forcing environment and atmospheric conditions.

Correlation with cloud top temperature (CTT)

• Observation: both CO_2 ($r = 0.31$) and CH_4 ($r = 0.32$) showed a positive correlation with CTT.

• Interpretation and essence: this is a key indicator of the greenhouse effect in action.

(1) CO_2 and CH_4 are well-mixed greenhouse gases that absorb thermal infrared radiation emitted by the Earth's surface and the atmosphere.

(2) This absorption warms the atmospheric layer where it occurs.

(3) Clouds form at altitudes where the temperature drops to the dew point. If the entire lower atmosphere (the troposphere) is warmer due to increased GHG concentrations, the cloud formation altitude might shift, or the cloud tops might be warmer.

(4) A higher cloud.

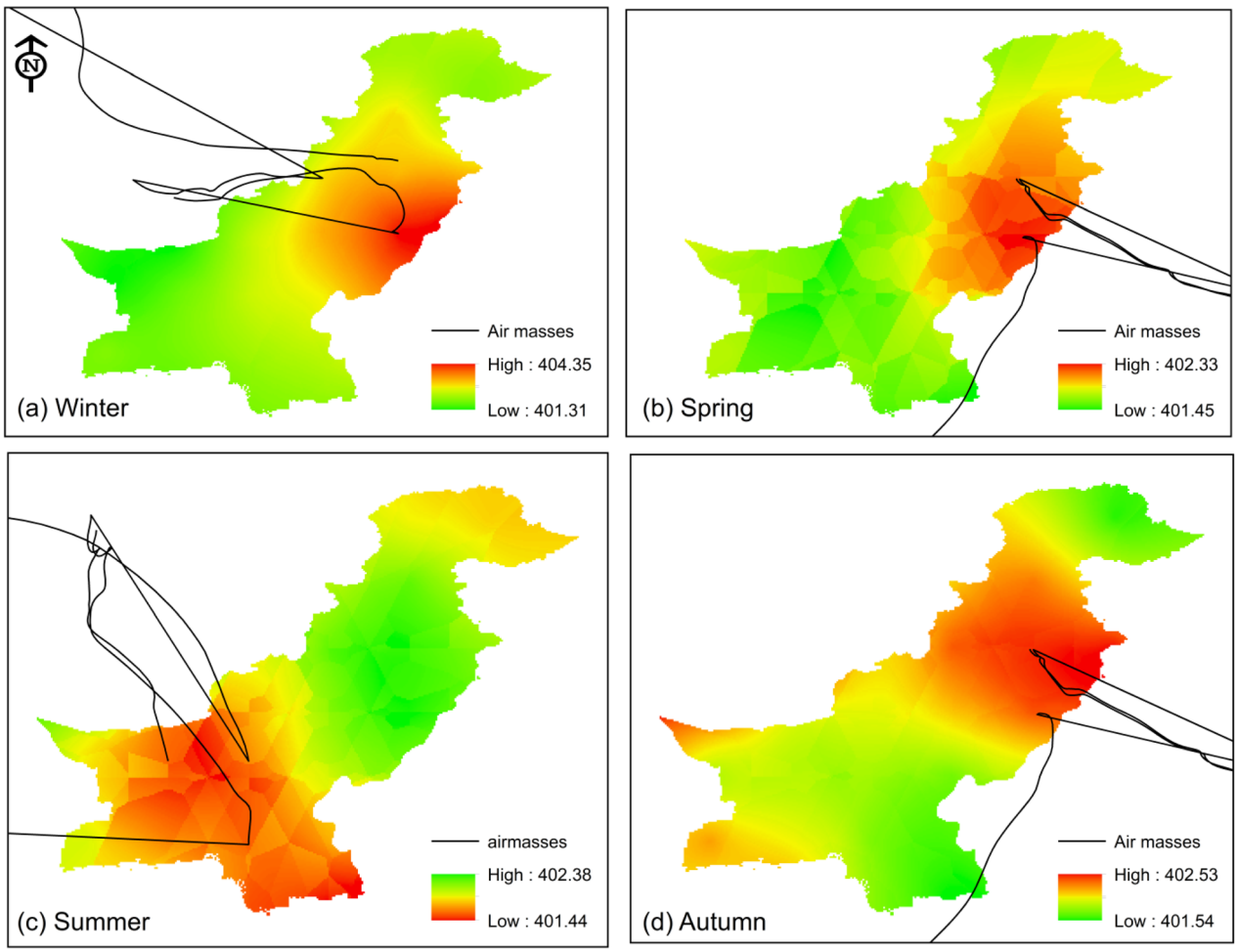

Fig. 11 Seasonal spatial distribution of mid-tropospheric CO_2 (ppbv) during four seasons, including (a) winter (December–February), (b) spring (March–May), (c) summer (June–August), and (d) autumn (September–November), along with 3 days air masses reaching Pakistan observed at 1000 m from the ground level during the study period.

Influence of air masses

Currently, air mass back trajectories are used to investigate the long- and short-range transportation of pollutants from one region of the earth to another region.[43,45] Using the Hybrid Single Particle Lagrangian Integrated Trajectory (HYSPLIT) model, the backward trajectories arriving at Pakistan were examined during the entire study period (2002–2017) at 1000 m above ground level.[46] In the current study, the HYSPLIT model shows the source of different backward trajectories of air masses from multiple regions reaching the study location, as shown in Fig. 11 and 12.

Fig. 11 (a) and (b) show the three-day back trajectory analysis of air masses at a height of 1000 m above the ground surface during the study period (2002–2017). The three-day back trajectories were calculated and clustered into four seasons for each entire study period (2002–2017) over Pakistan. It is clear from Fig. 11 that most of the source regions lie in the Middle East, arising from Egypt, Saudi Arabia, Iraq, Iran, *etc.*, and travel long distances to reach the receptor region, Pakistan. However, air masses also arise from central Asia from Turkmenistan and Uzbekistan and travel through Afghanistan to reach Pakistan. Air masses also arise from neighboring countries, such as India.

Middle Eastern countries are some of the strongest GHG emitters in the world.[47] In particular, Saudi Arabia is the largest producer and exporter of petroleum products, and 90% of its revenue relies on oil and petroleum-related industries.[48] In addition, the Peninsula (Iraq, Bahrain, Kuwait, Saudi Arabia, *etc.*) is considered a hotspot for the emission of GHGs due to vast oil and natural gas reserves and industries.[4] Moreover, in Iraq, the total CO_2 emission increased by 300% from fuels that are roughly 14 000 Gg and 58 000 Gg from 1990 to 2017.[9] In addition, the Egyptian share of GHG emissions to the global atmosphere increased from 0.4% in 2000 to 0.6% in 2016.[49] The air masses from these regions traveled through Iran and Afghanistan to reach Pakistan. Iran is ranked 7th in terms of CO_2 emissions resulting from fuel combustion in the world.[50] The main sources of CO_2 and CH_4 emissions are various sectors of energy production, agriculture, livestock, forestry, and waste. Moreover, in Afghanistan, coal burning is the major cause of GHG emissions, and over 70% of household energy is used to heat space and water. In Kabul, on average, each family produces 4062 kilograms of greenhouse gases (CO_2, NO_2 and CH_4), and concerning this value, approximately 2.39 million tons of GHG are

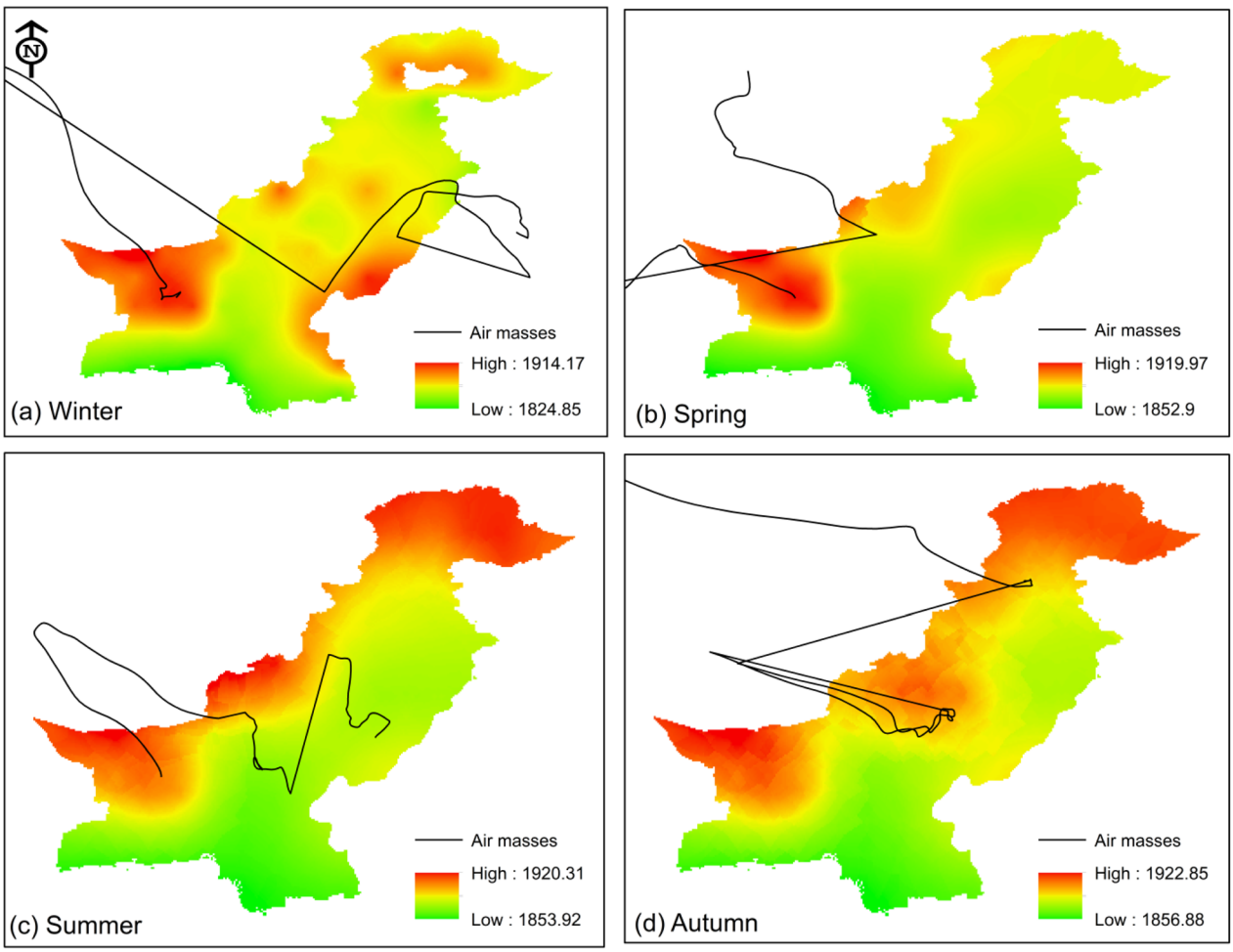

Fig. 12 Seasonal spatial distribution of mid-tropospheric CH_4 (ppbv) during four seasons, including (a) winter (December–February), (b) spring (March–May), (c) summer (June–August), and (d) autumn (September–November), along with 3 days air masses reaching Pakistan observed at 1000 m from the ground level during the study period.

Table 5 Quantitative performance metrics of each model during the training fit

Model	MSE	RMSE	MAE	R^2	MAPE
Linear regression	0.2101	0.4584	0.3714	0.9977	0.10%
Exponential smoothing	0.2101	0.4584	0.3714	0.9977	0.10%
ARIMA	8652.3921	93.0182	23.9110	−91.8053	6.42%
SARIMA	8652.3921	93.0182	23.9110	−91.8053	6.42%
LSTM	0.9590	0.9793	0.7783	0.9840	0.20%

emitted in one month during winter.[51] As shown in Fig. 12, some of the air masses arise from central Asia, including Turkmenistan and Azerbaijan. Turkmenistan is one of the few countries with an entire dependence on fossil fuels, with the sixth-largest natural gas reserve in the world. 99% of the electricity in the country is provided by natural gas-fired power plants.[52] Similarly, the economy of Azerbaijan is also significantly based on oil production.[53] The air masses from central Asia and Middle Eastern regions traveled through Afghanistan and reached Pakistan and contributed to locally emitted CH_4 and CO_2 to elevate their concentration in the regional troposphere.

CO_2 and CH_4 models of forecasting

In the current study, five forecasting models were evaluated based on predicting the annual concentrations of carbon dioxide (CO_2) and methane (CH_4) in the atmosphere between 2002 and 2017 using Linear Regression, Exponential Smoothing (ETS), Autoregressive Integrated Moving Average (ARIMA), Long Short-Term Memory (LSTM), and Seasonal Autoregressive Integrated Moving Average (SARIMA) models.

To predict atmospheric CO_2 and CH_4 concentrations from 2002 to 2017, we evaluate the performance of five forecasting models: Linear Regression, Exponential Smoothing (ETS), ARIMA, LSTM, and SARIMA. The tuning of the Hyperparameter is conducted for each model.

LSTM

• Architecture: LSTM single layer is followed by a dense output layer.

• Hyperparameters: we experimented with different settings. The last model had 50 units in the LSTM layer at a learning rate of 0.01 and 1000 epochs. The predictive data used a rolling window of the past 3 years.

Training: the Adam optimizer and Mean Squared Error (MSE) were used as the loss function to train the model. Even with tuning, the model never converged to a solution that was better than the linear trend, which means that it was overfitting, and the model was fundamentally incorrect in its approach to the data, which was highly linear.

ARIMA/SARIMA

• Model selection: the optimal model was chosen using the Akaike Information Criterion (AIC).

Hyperparameters of CO_2: the optimal performance of the ARIMA was ARIMA (1,1,1), meaning one autoregressive term, one degree of differencing, and one moving average term.

Smart parameters of SARIMA: we tested seasonal terms (*e.g.*, SARIMA (1,1,1) (1,1,1,12)), but there was no significant seasonal model in the annual aggregated data, showing that SARIMA was an overly complicated selection.

Linear regression and ETS

They are simpler models in which hyperparameters that must be tuned are not present within the model (*e.g.*, ETS model, additive error, trend, and seasonality). It is this simplicity that is their strength.

Best-fitting model results with statistical results

As illustrated in Tables 5–7, the most meaningful statistical findings are the following models:

• Linear regression is the clearly best model in CH_4. It gave the fewest errors on the test forecast (2018–2024) with an MAE of 2.123 ppb, RMSE of 2.456 ppb, and MAPE of 0.12%. The trend is overwhelmingly linear as it almost explains everything in the historical data ($R^2 = 0.9977$).

• In the case of CO_2, ARIMA (1, 1, 1) gave the best projections. It performed better during the test period, as it gave the lowest RMSE (2.7023) and the highest R2 (0.4818), which means that it could capture the small autocorrelation structure of the CO_2 data that a pure linear trend failed to capture.

The findings summarize that linear regression is the choice of chart to use in CH_4 prediction, and ARIMA is the choice of chart in predicting CO_2 in the case of this data. The LSTM

Table 6 Quantitative performance metrics of each model while forecasting CO_2 from 2028 to 2024

Model	MSE	RMSE	MAE	R^2	MAPE
LSTM	9.7485	3.1223	2.7073	0.3082	0.65%
ARIMA	7.3027	2.7023	2.6265	0.4818	0.63%
Exponential smoothing	12.3441	3.5134	3.4823	0.1240	0.84%
Linear regression	12.3441	3.5134	3.4823	0.1240	0.84%

Table 7 Quantitative performance metrics of each model while forecasting CH_4 from 2028 to 2024

Model	MAE	RMSE	MAPE
Linear regression	2.123	2.456	0.12%
ETS	3.215	3.678	0.18%
ARIMA	4.892	5.234	0.27%
ARIMA (1,1,1)	3.956	4.312	0.22%
LSTM	5.678	6.123	0.31%

model, which is the most complex, still performed the worst, which confirms our assumption that easier models are more effective in this case.

Characteristics and model fitting of data

The two gases (Fig. 13 and 14) showed a strong linear, positive rise over time with little noise or seasonality in the annual aggregate data. This inherent property was the major determinant of model performance, as indicated in the training fit figures (*e.g.*, Fig. 15 and 16) and measured in Table 5.

Linear regression showed an almost perfect fit using the historical data of the two gases, with an R^2 of 0.9977 for CO_2. This means that the simple linear trend describes more than 99.7 percent of the variance in the data, and more complicated models are not needed to describe the historical pattern. The steady annual growth (about 2.0–2.3 ppm per year of CO_2) is best fitted to a linear model.

More sophisticated models, such as SARIMA (seasonality) and LSTM (complex non-linearities), did not manage to do so on the training data. The benefit of their added complexity was not significant, and, as is usual with parsimonious data, they introduced a risk of overfitting.

Performance and model comparison forecasting

Linear regression continued performing better in the near-term forecasting task (2018–2024) with respect to CH_4.

CO_2 forecasting

CO_2 results, illustrated in Table 6 and Fig. 17, were more subtle. Linear regression optimally fits the trend in history, but the ARIMA model was the best in terms of forecasting performance during the test period, with the lowest RMSE (2.7023) value and the highest R^2 value (0.4818). This indicates that the trend is linear, but the explicit modelling and extrapolation of the autocorrelation structure in the time series (*e.g.*, integration of past values and errors) using the ARIMA model had a small effect on forecast performance relative to linear extrapolation alone in the case of CO_2.

It is worth noting that the LSTM model performed poorly for both gases. This is typical when small and clean datasets are employed, which are highly linear because LSTMs require large amounts of data to learn more complicated patterns and can be easily outperformed by simpler and more statistically suitable models.

For CH_4 forecasting

Linear regression was clearly the superior model, as illustrated in Table 7 and Fig. 18. It recorded the lowest error values (MAE: 2.123 ppb, RMSE: 2.456 ppb, MAPE: 0.12%), which were far better than all the other models, including ETS and ARIMA. This proves that the increase in atmospheric methane over the future prognosis still takes a strong and consistent linear form due to consistent anthropogenic emissions.

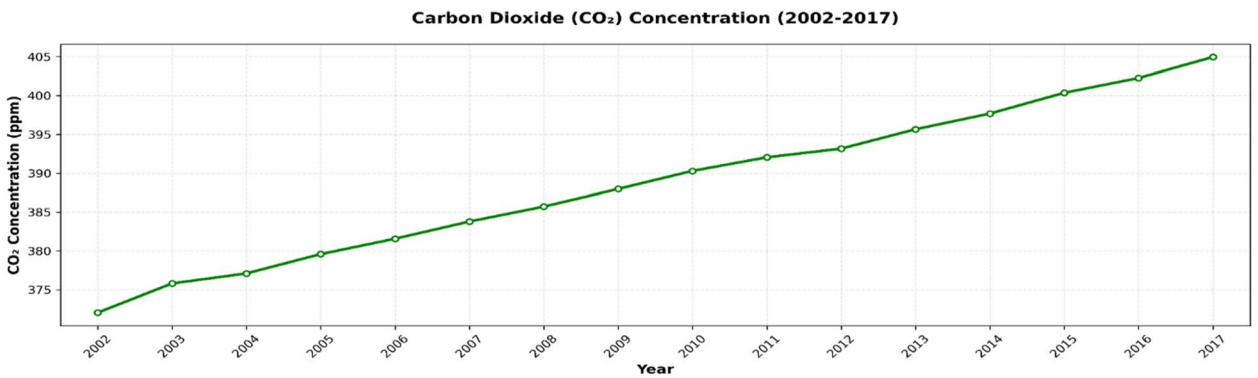

Fig. 13 Carbon dioxide (CO_2) concentration from 2002–2017.

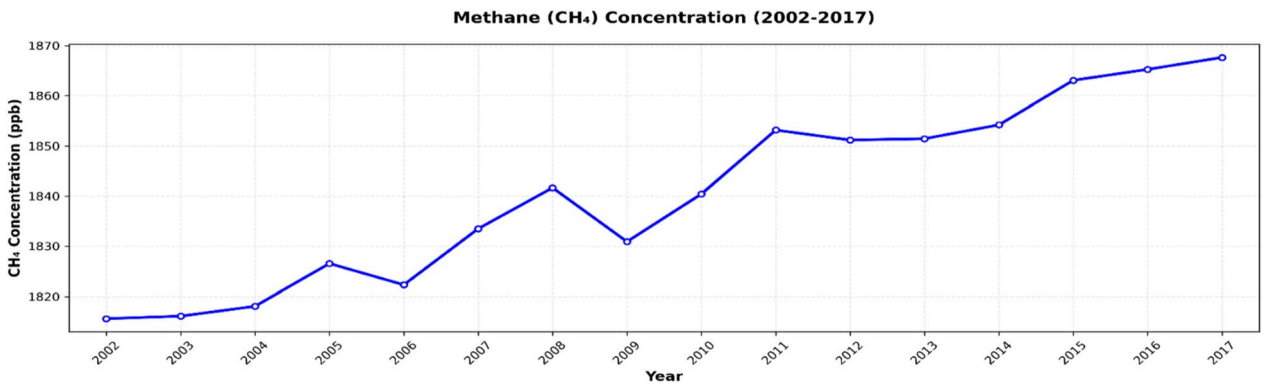

Fig. 14 Methane (CH_4) concentration from 2002–2017.

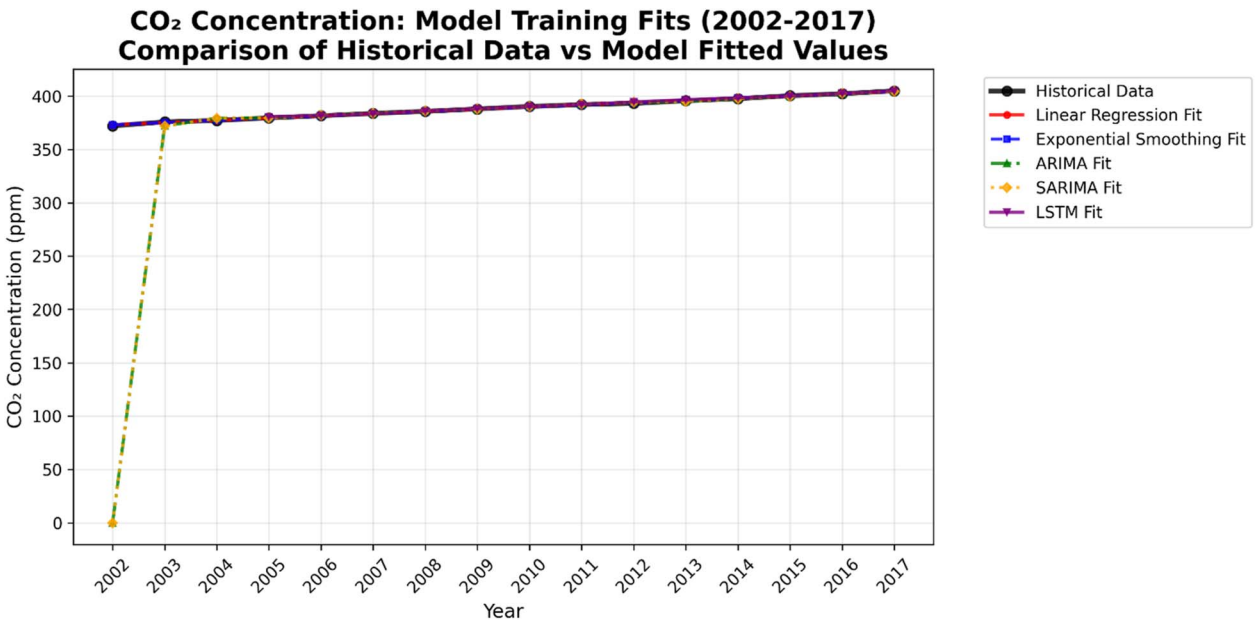

Fig. 15 Comparison of the training fits of different models using the CO_2 historical data.

Recommendations

The most important result of this study is that the characteristics of the data significantly affect the performance of the model. In these particular annual concentration data, which are non-seasonal, short, and have a strong linear trend, the simplest model (linear regression) was either optimal or highly competitive. Thus, in light of our findings, we advise the following:

(1) Because of its remarkable accuracy, ease of use, interpretability, and low processing cost, linear regression should be the model of choice for operational forecasting of CH_4 with this type of data.

(2) An ARIMA model should be considered for CO_2 forecasting since it captured the trend and autocorrelation well and produced the most accurate forecasts in our test scenario.

Significance

The environmental science community can benefit greatly from this study since it shows that reliable and precise operational forecasts of CO_2 and CH_4 can be produced without the computational cost and data needs of sophisticated machine learning models like LSTM. Clearly, fact-based recommendations for model selection for regional GHG trend predictions are provided in our analysis.

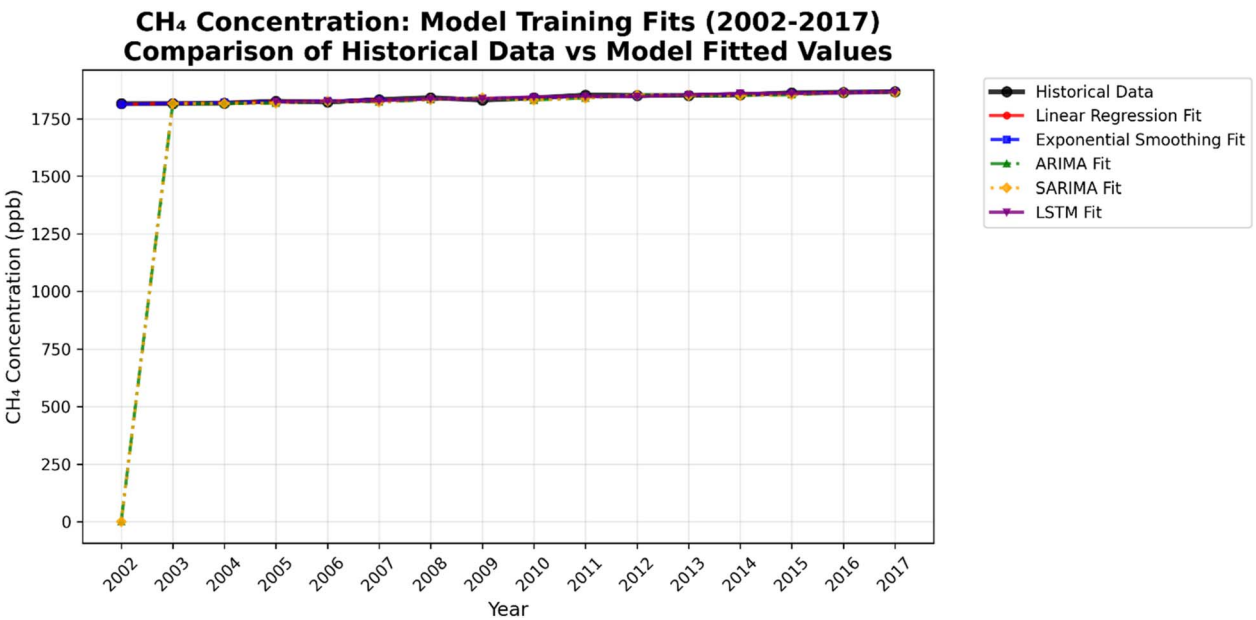

Fig. 16 Comparison of the training fits of different models using the CH_4 historical data.

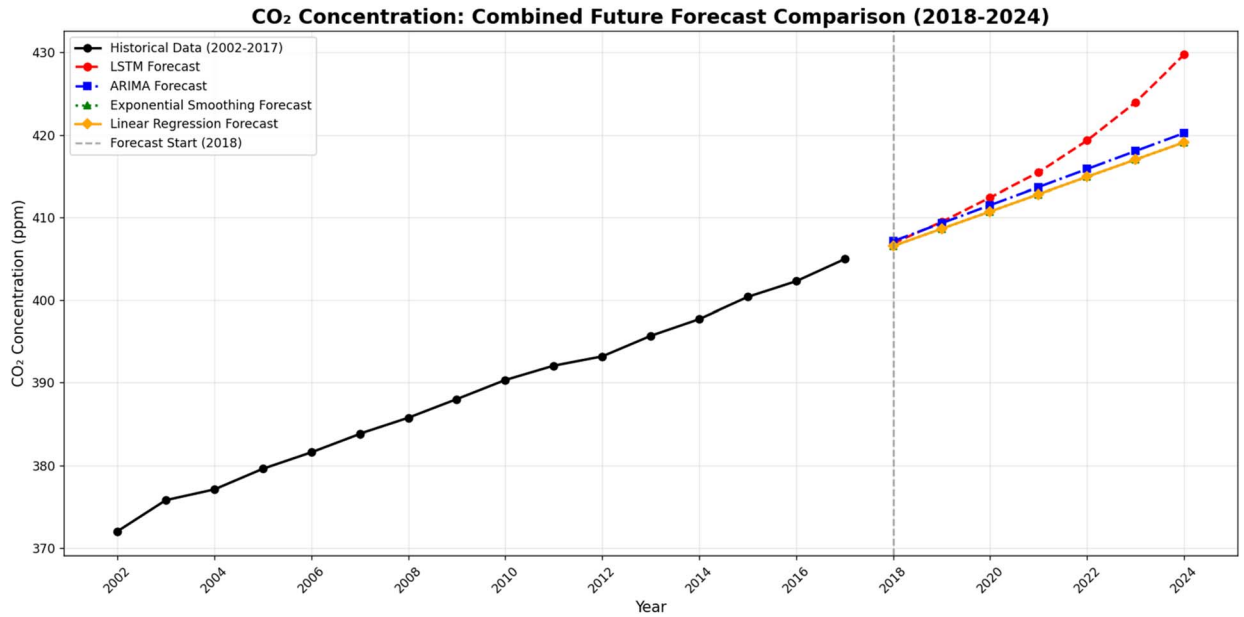

Fig. 17 Comparison of different models while forecasting CO_2 from 2018 to 2024.

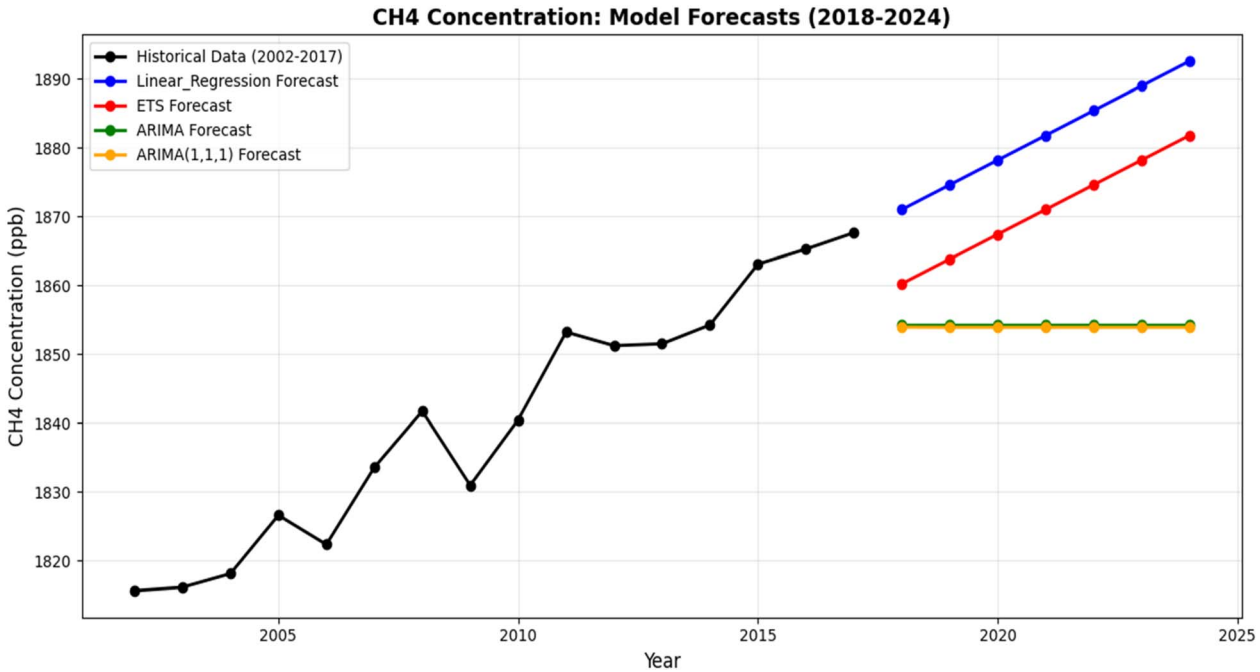

Fig. 18 Comparison of different models for forecasting CH_4 from 2018–2024.

(1) Finding the most realistic model for predicting these particular GHG trends was the goal.

(2) The concept of parsimony is the main finding: the most effective model is the simplest one (linear regression for CH_4 and ARIMA for CO_2), as adding complexity (LSTM and SARIMA) had no advantage and frequently resulted in worse performance.

(3) We specifically address the reasons why complicated models do not work, such as LSTM's requirement for huge datasets to identify patterns that are already well captured by a straightforward linear trend.

Conclusions

This study is an in-depth examination of tropospheric CO_2 and CH_4 changes in Pakistan between 2002 and 2017 using AIRS satellite data, which has provided vital information about seasonal patterns, climatic factors, and human effects. Key findings include the following:

➢ CO_2 maxima in May (389 ± 8 ppmv) resulted from increased biomass burning, soil respiration, and pre-monsoon agricultural activities, and minima in October (386 ± 8 ppmv) occurred after photosynthetic uptake during the monsoons.

➢ CH_4 peaks in August (1876 10 ppbv) with wetlands and rice planting during the monsoon, and the lowest concentrations occur in April (1820 21 ppbv) with decreased photochemical activity.

➢ Both gases are characterised by a high rate of increase: CO_2 increasing by 2.1 ppmv/year and CH_4 increasing by 3.5 ppbv per year over 15 years, corresponding to total increases of 8.6 and 2.9 percent, respectively.

➢ Sudden shifts observed through the Mann–Kendall test (CO_2 in 2009, CH_4 in 2007–2014) are consistent with the increased anthropogenic effects (industrial expansion, deforestation, and burning of fossil fuels).

➢ CO_2 has a negative relationship with NDVI ($r = -0.50$) and precipitation, showing the importance of vegetation and monsoonal uptake in concentration control.

➢ CH_4 exhibits very positive correlations with NDVI ($r = 0.64$) and temperature ($r = 0.60$), with both microbial activity and agricultural emissions being dependent on temperature.

➢ Both gases affect radiative forcing, with CO_2 and CH_4 having cloud top temperature and cloud fraction relationships, respectively, of $r = 0.31$ and $r = -0.20$, highlighting the climatic feedback processes of the two gases.

➢ The HYSPLIT trajectory analysis indicates transboundary Middle East (oil/gas industries) and Central Asia (fossil fuel dependence) contributions to the problem of local agriculture, transportation, and biomass burning emissions.

➢ Increased surveillance: increased ground-based and satellite monitoring to measure emission hotspots and model climates.

➢ Emission control: strengthening of the emission control of industries and vehicles, use of renewable energy, and sustainable agricultural methods (*e.g.*, alternate wetting/drying in rice fields).

➢ Regional cooperation: collaborate with other neighbouring countries to deal with transboundary pollution by working together on similar climate programmes.

In addition, it was observed that simple statistical models (linear regression of CH_4 and ARIMA of CO_2) performed better than more complicated models, such as LSTM, in the scenario of strongly linear trends of GHG. This offers an excellent, cost-effective model in which policymakers and scientists can project future GHG concentrations and evaluate scenarios for the mitigation of emissions without the complexity and obscurity of computationally demanding models.

Author contributions

Conceptualization: BZ, KA, AD, RI, IA, AEMAM, MA, and ML; data curation: BZ, AD, and KA; formal analysis: BZ, KA, AD, RI, IA, AEMAM, MA, and ML; investigation: BZ; methodology, BZ, AD, and KA; project administration: BZ, AD, and KA; resources: BZ, KA, AD, RI, IA, and AEMAM; software: BZ, KA, AD, RI, IA, and AEMAM; supervision: KA; validation, BZ, KA, AD, RI, IA, and AEMAM; visualization: BZ, KA, AD, RI, IA, and AEMAM; writing – original draft: BZ; and writing – review & editing: BZ, KA, AD, RI, IA, AEMAM, MA, and ML. All the authors read and approved the final submission.

Conflicts of interest

There are no conflicts to declare.

Data availability

Data will be made available from the corresponding author on reasonable request.

Acknowledgements

The scientific teams of NASA's AIRS and MODIS sensors are gratefully acknowledged for making the datasets used in the present study available online. We are also grateful to the NOAA ARL for computing backward trajectories through the HYSPLIT model and the Pakistan Meteorological Department for providing the meteorological data. The authors would like to thank the anonymous reviewers for their critical comments and constructive suggestions in improving the manuscript.

Notes and references

1 S. Fawzy, A. I. Osman, J. Doran and D. W. Rooney, *Environ. Chem. Lett.*, 2020, **18**, 2069–2094, DOI: 10.1007/s10311-020-01039-0.

2 IPCC, in *Climate Change 2021: the Physical Science Basis. Contribution of Working Group I to the Sixth Assessment Report of the Intergovernmental Panel on Climate Change*, ed. V. Masson-Delmotte, P. Zhai, A. Pirani, S. L. Connors, C. Péan, S. Berger, N. Caud, Y. Chen, L. Goldfarb and M. I. Gomis, et al., Cambridge University Press, Cambridge, United Kingdom and New York, NY, USA, 2021, DOI: 10.1017/9781009157896.

3 Ø. Hodnebrog, B. Aamaas, J. S. Fuglestvedt, G. Marston, G. Myhre, C. J. Nielsen, M. Sandstad, K. P. Shine and T. J. Wallington, *Rev. Geophys.*, 2020, **58**, e2019RG000691, DOI: 10.1029/2019RG000691.

4 M. Alcibahy, F. A. Gafoor, F. Mustafa, M. El Fadel, H. Al Hashemi, A. Al Hammadi and M. R. Al Shehhi, *Sci. Rep.*, 2025, **15**, 766, DOI: 10.1038/s41598-024-12345-0.

5 A. K. Patra, *Asian-Australas. J. Anim. Sci.*, 2014, **27**, 592–599, DOI: 10.5713/ajas.2014.r.01.

6 C. Le Quéré, R. M. Andrew, P. Friedlingstein, S. Sitch, J. Hauck, J. Pongratz, P. A. Pickers, J. I. Korsbakken, G. P. Peters, J. G. Canadell and A. Arneth, *Earth Syst. Sci. Data*, 2018, **10**, 2141–2194, DOI: 10.5194/essd-10-2141-2018.

7 G. L. Foster, D. L. Royer and D. J. Lunt, *Nat. Commun.*, 2017, **8**, 14845, DOI: 10.1038/ncomms14845.

8 M. Krishnapriya, R. K. Nayak, S. Allahudeen, A. Bhuvanachandra, V. K. Dadhwal, C. S. Jha, M. V. R. Sheshasai, S. K. Sasmal and K. V. S. R. Prasad, *J.*

Earth Syst. Sci., 2020, **129**, 211, DOI: 10.1007/s12040-020-01476-z.

9 F. Abed, J. Rajab, I. Abdulfattah and H. San Lim, *Atmos. Pollut. Res.*, 2024, **15**, 102293, DOI: 10.1016/j.apr.2023.102293.

10 M. A. Khaliq, F. Mustafa, S. U. Rehman, M. Shahzaman, Z. Javed, M. Sagir, S. Bashir and H. Zuo, *Sci. Total Environ.*, 2024, **922**, 171311, DOI: 10.1016/j.scitotenv.2024.171311.

11 P. I. Palmer, Y. Zheng, T. D. Sharkey, J. D. Maasakkers, H. Boesch, R. J. Parker, H. L. Deutch and J. W. C. White, *Nat. Rev. Earth Environ.*, 2024, **5**, 87–102, DOI: 10.1038/s43017-023-00503-z.

12 S. Kirschke, P. Bousquet, P. Ciais, M. Saunois, J. G. Canadell, E. J. Dlugokencky, P. Bergamaschi, D. Bergmann, D. R. Blake, L. Bruhwiler, P. Cameron-Smith, S. Castaldi, F. Chevallier, L. Feng, A. Fraser, M. Heimann, E. L. Hodson, S. Houweling, B. Josse, P. J. Fraser, P. B. Krummel, J.-F. Lamarque, R. L. Langenfelds, C. Le Quéré, V. Naik, S. O'Doherty, P. I. Palmer, I. Pison, D. Plummer, B. Poulter, R. G. Prinn, M. Rigby, B. Ringeval, M. Santini, M. Schmidt, D. T. Shindell, I. J. Simpson, R. Spahni, L. P. Steele, S. A. Strode, K. Sudo, S. Szopa, G. R. van der Werf, A. Voulgarakis, M. Weele, R. F. Weiss, J. E. Williams and Z. Guang, *Nat. Geosci.*, 2013, **6**, 813–823.

13 K. Tawiah, M. Daniyal and M. Qureshi, *J. Environ. Public Health*, 2023, **2023**, 5903362, DOI: 10.1155/2023/5903362.

14 S. K. Goroshi, R. P. Singh, S. Panigrahy and J. S. Parihar, *Indian Soc. Remote. Sens.*, 2011, **39**, 315–321, DOI: 10.1007/s12524-011-0115-1.

15 I. Mahmood, M. F. Iqbal, M. I. Shahzad, A. Waqas and L. Atique, *Int. Lett. Nat. Sci.*, 2016, **58**, 35–41, DOI: 10.18052/www.scipress.com/ILNS.58.35.

16 N. An, F. Mustafa, L. Bu, M. Xu, Q. Wang, M. Shahzaman, M. Bilal, S. Ullah and Z. Feng, *Remote Sens.*, 2022, **14**(22), 5882, DOI: 10.3390/rs14225882.

17 M. Noman, A. R. Ghazali, A. A. Mahesar, S. A. A. S. Naqvi and M. F. D. Al-Khaldi, *Environ. Sci.:Adv.*, 2024, **3**, 580–591, DOI: 10.1039/D3VA00298A.

18 B. Zeb, K. Alam, A. Sorooshian, F. Chishtie, I. Ahmad and H. Bibi, *J. Atmos. Sol.-Terr. Phys.*, 2019, **186**, 35–46, DOI: 10.1016/j.jastp.2019.02.005.

19 M. T. Chahine, L. Chen, P. Dimotakis, X. Jiang, Q. Li, E. T. Olsen and Y. L. Yung, *Geophys. Res. Lett.*, 2008, **35**, L17801, DOI: 10.1029/2008GL035203.

20 A. Singh, C. P. Pandey, H. Nandan and P. Semwal, *Indian Soc. Remote. Sens.*, 2023, **51**, 1553–1564, DOI: 10.1007/s12524-023-01724-x.

21 G. Sreenivas, P. Mahesh, J. Subin, A. L. Kanchana, P. V. N. Rao and V. K. Dadhwal, *Atmos. Chem. Phys.*, 2016, **16**, 3953–3967, DOI: 10.5194/acp-16-3953-2016.

22 K. Sreenivas, V. K. Dadhwal, S. Kumar, G. S. Harsha, T. Mitran, G. Sujatha and T. Ravisankar, *Geoderma*, 2016, **269**, 160–173, DOI: 10.1016/j.geoderma.2016.02.004.

23 H. B. Mann, *Econometrica*, 1945, **13**, 245–259, DOI: 10.2307/1907187.

24 M. G. Kendall, *Rank Correlation Methods*, Griffin, London, 1975.

25 R. Sneyers, *Environmetrics*, 1997, **8**, 517–527, DOI: 10.1002/(SICI)1099-095X(199709/10)8:5<517::AID-ENV267>3.0.CO;2-P.

26 Y. Q. Wang, X. Y. Zhang and R. R. Draxler, *Environ. Model. Softw.*, 2010, **24**, 938–939, DOI: 10.1016/j.envsoft.2009.01.004.

27 T. G. Gilmanov, D. A. Johnson, N. Z. Saliendra, K. Akshalov and B. K. Wylie, *J. Environ. Manage.*, 2004, **33**, S492–S508, DOI: 10.1007/s00267-003-9150-1.

28 S. X. Fang, L. X. Zhou, P. P. Tans, P. Ciais, M. Steinbacher, L. Xu and T. Luan, *Atmos. Chem. Phys.*, 2014, **14**, 2541–2554, DOI: 10.5194/acp-14-2541-2014.

29 X. Jing, J. Huang, G. Wang, K. Higuchi, J. Bi, Y. Sun and T. Wang, *Atmos. Chem. Phys.*, 2010, **10**, 8205–8218, DOI: 10.5194/acp-10-8205-2010.

30 Z. Ul Haq, S. Tariq and M. Ali, *J. Atmos. Sol.-Terr. Phys.*, 2015, **135**, 161–173, DOI: 10.1016/j.jastp.2015.11.004.

31 J. Kuttippurath, R. Peter, A. Singh and S. Raj, *iScience*, 2022, **25**, 105328, DOI: 10.1016/j.isci.2022.105328.

32 L. Cao, X. Chen, C. Zhang, A. Kurban, J. Qian, T. Pan, Z. Yin, X. Qin, F. U. Ochege and P. D. Maeyer, *Remote Sens.*, 2019, **11**, 94, DOI: 10.3390/rs11010094.

33 C. Wei, M. Wang, Q. Fu, C. Dai, R. Huang and Q. Bao, *Atmos. Res.*, 2020, **235**, 104759, DOI: 10.1016/j.atmosres.2019.104759.

34 K. R. Kumar, J. V. Revadekar and Y. K. Tiwari, *Sci. Total Environ.*, 2014, **476–477**, 79–89, DOI: 10.1016/j.scitotenv.2013.12.090.

35 A. Metya, A. Datye, S. Chakraborty, Y. K. Tiwari, D. Sarma, A. Bora and N. Gogoi, *Sci. Rep.*, 2021, **11**, 2931, DOI: 10.1038/s41598-021-82352-8.

36 O. Schneising, M. Buchwitz, J. P. Burrows, H. Bovensmann, P. Bergamaschi and W. Peters, *Atmos. Chem. Phys.*, 2009, **9**, 443–465, DOI: 10.5194/acp-9-443-2009.

37 S. K. Goroshi, R. P. Singh, S. Panigrahy and J. S. Parihar, *Indian Soc. Remote. Sens.*, 2011, **39**, 315–321.

38 S. Hayashida, A. Ono, S. Yoshizaki, C. Frankenberg, W. Takeuchi and X. Yan, *Remote Sens. Environ*, 2013, **139**, 246–256.

39 A. Gaur, S. N. Tripathi, V. P. Kanawade, V. Tare and S. P. Shukla, *J. Atmos. Chem.*, 2014, **71**, 283–301, DOI: 10.1007/s10874-014-9295-8.

40 T. Nishanth, K. M. Praseed, M. K. S. Kumar and K. T. Valsaraj, *Aerosol Air Qual. Res.*, 2014, **14**(3), 1074–1088, DOI: 10.4209/aaqr.2013.10.0315.

41 M. Kavitha and P. R. Nair, *Atmos. Environ.*, 2016, **131**, 316–325, DOI: 10.1016/j.atmosenv.2016.02.017.

42 M. Pathakoti, S. Gaddamidi, B. Gharai, P. Sudhakaran Syamala, P. V. N. Rao, S. B. Choudhury, K. V. Raghavendra and V. K. Dadhwal, *Polar Res.*, 2018, **37**, 1442072, DOI: 10.1080/17518369.2018.1442072.

43 M. Nyasulu, M. M. Haque, K. R. Kumar, N. Banda, B. Ayugi and M. J. Uddin, *Atmos. Pollut. Res.*, 2021, **12**, 125–135, DOI: 10.1016/j.apr.2020.10.016.

44 P. Mahesh, N. Sharma, V. K. Dadhwal, P. V. N. Rao, B. V. Apparao, A. K. Ghosh, K. Mallikarjun and M. M. Ali,

J. Earth Sci. Clim. Change, 2014, **5**, 1000199, DOI: 10.4172/2157-7617.1000199.

45 R. Boiyo, K. R. Kumar, T. Zhao and Y. Bao, *Atmos. Environ.*, 2017, **152**, 298–313, DOI: 10.1016/j.atmosenv.2016.12.045.

46 R. R. Draxler and G. D. Rolph, *HYSPLIT (Hybrid Single-Particle Lagrangian Integrated Trajectory) Model*, NOAA Air Resources Laboratory, 2013, available at https://www.ready.arl.noaa.gov/HYSPLIT.php.

47 M. Liu, A. R. van der, M. van Weele, L. Bryan, H. Eskes, P. Veefkind and J. Ding, *Atmos. Meas. Tech.*, 2024, **17**, 5261–5277, DOI: 10.5194/amt-17-5261-2024.

48 S. M. Rahman and A. N. Khondaker, *Renewable Sustainable Energy Rev.*, 2012, **16**, 2446–2460, DOI: 10.1016/j.rser.2012.01.075.

49 M. Fahmy, M. M. Mahdy, H. Rizk and M. F. Abdelaleem, *Ain Shams Eng. J*, 2018, **9**, 2599–2607, DOI: 10.1016/j.asej.2017.10.007.

50 M. Ahmadi, M. Rozkhosh and N. A. Jaafarzadeh Haghighifard, *Environ. Health Eng. Manage. J.*, 2014, **1**, 29–35, DOI: 10.15171/EHEM.2014.05.

51 N. A. Rahmany and M. H. Patmal, *Int. J. Innov. Res. Sci. Stud*, 2021, **4**, 53–61, DOI: 10.53894/ijirss.v4i2.49.

52 R. Satymov, D. Bogdanov and C. Breyer, *IEEE Access*, 2021, **9**, 13590–13611, DOI: 10.1109/ACCESS.2021.3051563.

53 N. Vidadili, E. Suleymanov, C. Bulut and C. Mahmudlu, *Renewable Sustainable Energy Rev.*, 2017, **80**, 1153–1161, DOI: 10.1016/j.rser.2017.05.168.